

Measuring the Optical Properties of Human Muscle Tissue using Time-of-Flight Spectroscopy in the Near Infrared

Master's Thesis
by
Staffan Strömblad

Lund University
Faculty of Engineering, LTH
January 2015

Supervisors:
Dmitry Khoptyar,
Stefan Andersson-Engels



LUND
UNIVERSITY

Lund Reports on Atomic Physics, LRAP-498

Abstract

Optical spectroscopy is commonly used in technology and science today. The presence and concentration of a substance can be determined by its spectral signature, the typical wavelengths that are absorbed (or emitted) by the atoms or molecules. Standard absorption spectroscopy requires that the substance is clear and that the optical path-length is known to obtain quantitative information. Unfortunately in many materials, such as human tissue or pharmaceutical tablets, there are also a strong scattering of light which complicates measurements. The path-length of the light is now no longer known and the intensity of the detected light can in many cases be more affected by high scattering than by the absorption values.

One method to separate these two values are photon Time-of-Flight Spectroscopy (TOFS). By sending many short light pulses through a sample, and recording the time for a single photon to arrive at our detector for each pulse, we can build a histogram that represents the broadening of the light pulse that is determined by both the scattering and absorption. By fitting computer generated theoretical curves against the recorded histogram, we can extract the values for absorption and scattering from the curve with the best fit.

The Biophotonics group at the department of Physics at Lund University has implemented a system that can deliver continuous absorption/scattering spectra from 500 nm to 1400 nm. It uses a broadband laser as source and tunable optical filters to select narrow wavelength bands for measurements. In this thesis we expanded the set-up with a new laser source and new filters. We performed tests comparing measurements using the new filter with results from the old system. We could show that the new filter gave better results, due to the sharper line width of the output light pulse.

Study were also conducted on the absorption and scattering spectra of muscle tissue in the near infrared, between 650 nm and 1350 nm, probing the lower left arm of a volunteer. This was performed by positioning two optical fibres against the skin, sending light in with one and measuring the scattered light arriving at the second. The results are shown to be comparable to other studies done for wavelengths up to 1000 nm, and give new data up to 1350 nm that is consistent with the properties of the main absorbing components in this range, lipids and water. One uncertainty that appear in the results are due to the compression of the tissue by the fibres, this is something that should be addressed in repeat measurement that where not possible to perform in this study.

Populärvetenskaplig sammanfattning

Att använda hur ljus absorberas för att ta reda på något om ett ämne är inget konstigt, vi har alla gjort det. När vi blandar ett glas saft tittar vi på färgen och kan säga av erfarenhet hur stark den är. Precis på samma sätt fungerar absorptionsspektroskopi, genom att titta på hur mycket ljus som passerar genom ett material kan vi bestämma koncentrationen av ett ämne vi är intresserade av, om vi mäter hur mycket ljus detta ämne absorberar och vet hur lång väg genom materialet som ljusstrålen går. Olika färger på ljuset, olika våglängder, absorberas olika mycket av ämnen, och detta kan användas för att bestämma vad som finns i det vi tittar på. På så sätt kan vi enkelt skilja på gul apelsinsaft och röd jordgubbssaft.

För saft är detta enkelt, men det blir mycket svårare för till exempel mjölk. Anledningen till att mjölk är vit är nämligen att allt ljus som kommer in i mjölken sprids, det studsar runt mellan små fettdroppar och luftbubblor. Detta gör att det är omöjligt att veta hur lång sträcka ljuset gått igenom mjölken, för vi vet inte hur många gånger det ändrat riktning på vägen. Nu beror mängden ljus som passerar materialet på både spridningen och absorptionen, och vi måste ta hänsyn till bägge värden. Det går inte enkelt att skilja på olika mjölktyper bara genom att titta på dem.

Ett sätt att mäta både absorption och spridning som används i denna avhandling kallas photon Time-of-Flight Spectroscopy, pTOFS, där man mäter den tid det tar för enstaka ljuspartiklar, fotoner, att passera igenom materialet. Genom att göra många mätningar kan man bygga upp en graf som representerar den statistiska fördelningen av tiden det tar för fotonerna att passera, och formen på denna graf innehåller information om hur mycket absorption och spridning som ljuset utsatts för på sin väg. Genom att göra datorberäkningar där vi varierar spridning och absorption kan vi ta fram teoretiska grafer med kända värden. Sedan jämför vi datorgraferna med de uppmätta, och när vi hittar en som ser exakt likadan ut så kan vi läsa av värdena för absorption och spridning.

En typ av kraftigt spridande material är biologisk vävnad. Det finns redan många metoder att få fram information om vävnad, t.ex. röntgen, magnetkamera eller vävnadsprov. Fördelen med att använda ljus framför andra metoder är att det inte orsakar någon skada på vävnaden och det är relativt snabbt och billigt. Den stora nackdelen är att ljuset inte förmår tränga in så långt i vävnaden, typiskt nån millimeter till några centimeter beroende på vävnadstyp och ljusets våglängd.

Denna avhandling har som mål att mäta värden för absorption och spridning i mänsklig muskelvävnad för infrarött ljus. Detta har utförts med en pTOFS-uppställning på avdelningen för atomfysik vid Lunds Universitet. Först installeras nya delar för att få bättre ljusstyrka och vi utvärderar dessa, för att sedan mäta upp absorption och spridningsvärden för en muskel på en frivillig persons underarm. Resultaten visar att det är möjligt att använda metoden en bit in i det infraröda området, men sedan ökar absorptionen från vatten i vävnaden kraftigt och omöjliggör vidare mätning.

Contents

1	Introduction	1
1.1	Background	1
1.2	Aim of the thesis	1
1.3	Structure	1
2	Time of Flight Spectroscopy	3
2.1	Introduction	3
2.1.1	Absorption and scattering	3
2.1.2	Time of Flight Spectroscopy	4
2.2	Instrumental setup	6
2.2.1	Lasers	6
2.2.2	Filters	7
2.2.3	Detectors	7
2.3	Data handling	7
2.3.1	Diffusion theory	7
2.3.2	Monte Carlo simulations	7
2.4	Target setup	8
2.4.1	Tablet measurements	8
2.4.2	Muscle measurements	8
2.5	Measuring procedure	9
2.5.1	Measurements	10
3	Theory	11
3.1	Light propagation in turbid media	11
3.1.1	Absorption	11
3.1.2	Scattering	11
3.1.3	Scattering phase function	12
3.2	Radiative Transfer Equation	12
3.3	Diffusion model	14
3.4	Monte Carlo	15
3.5	Resolution effects	16
3.6	Biological tissue	16
3.6.1	Muscle tissue	17
3.6.2	In vivo measurements	17
4	Instrumental setup	19
4.1	Lasers	19
4.2	Filters	20
4.2.1	AOTF	20
4.2.2	LLTF	21
4.3	Fibres	21
4.4	Attenuators	21
4.5	Detectors	21
4.5.1	SPAD detector (400 - 1000 nm)	22
4.5.2	PMT detector (950 - 1400 nm)	22
4.6	TCSPC	22
4.7	Software	22
4.7.1	LUNDtofs program	23

4.7.2	Timeresolved v3	24
5	New system setup	25
5.1	Rebuilding old system	25
5.2	Installation of new components	25
5.3	10 W Laser SC-480-10	25
5.4	LLTF	26
5.4.1	General performance	27
5.4.2	BG36 measurements	28
5.4.3	N18ln2c measurements	28
5.5	Comparing systems	29
6	Muscle tissue measurement	31
6.1	Material and method	31
6.1.1	Data collecting and Evaluation	31
6.2	Results and discussion	32
6.2.1	Validating method	32
6.3	Optical properties above 1000 nm	34
6.3.1	Shorter fibre separation	35
6.3.2	10 mm spectra	38
7	Concluding remarks and Outlook	40
7.1	Aims	40
7.2	Outlook	41
7.3	Personal reflections	41
8	Acknowledgements	42
A	Detailed schematic of the setup	45

List of Figures

2.1	Part (a) shows different paths a photon can take. The time it takes for a photon to pass depends on the path. Those travelling relatively straight with few scattering events, will arrive earlier than those that scatter many times. Late photons will have a larger probability of being absorbed, as the absorption depends on the path length travelled. Some photons will be lost as they exit through the tissue boundary. Part (b) shows the statistical distribution for the photons and how the light pulse is broadened in time. [1]	4
2.2	The measured data and the time reference can be seen in the result of a model fit. The sharp peaks at 2 ns are the time reference pulse used to correct for any temporal shift. They should overlap, if they do not then the IRF data is shifted. Modified from [2]	5
2.3	Schematic arrangement of the pTOF spectrometer [3]	6
2.4	Sketch of the tablet holders, modified from [2]	8
2.5	Fibre holder with the two optical fibres	9
3.1	The Henyey-Greenstein phase function for different values of the scattering anisotropy g-factor. [5]	12
3.2	Terms included in the RTE; (a) radiance, (b) losses due to absorption or scattering, (c) gains from scattering, (d) sources. [6]	13
3.3	Tissue optical window. Modified from [9]	16
3.4	Absorption coefficient spectra of lipid, water, elastin, and collagen. [10]	17
3.5	Absorption spectra from forearm of two subjects with different fat layers. The muscle tissue properties are masked by the lipids in the skin, as the light will not penetrate deep enough [12].	18
4.1	The setup of the Photon Time of Flight system. A broadband laser is connected to a filter that is tunable to only let a selected wavelength pass. The pulse is then split into an Instrumental Response Function (IRF) and a Sample arm. After the light have passed the sample the two pulses are recombined and led to a single photon counting detector. A counting card record a histogram that is then sent to a controlling software program. Modified from [13].	19
4.2	Functional diagram of a supercontinuum fibre laser source. A Master fibre laser creates a light pulse of a fixed wavelength, that is amplified and sent to a Non-linear fibre where it is spectrally broadened. [8]	20
4.3	Principle of TCSPC. Repeating the same measurement several time and recording the time of a detected photon will create a histogram seen in (a) . Illustrated in (b) , the detection of photon will trigger charging of a capacitor, which is stopped with the arrival of a sync signal from the laser source. The voltage over the capacitor is proportional to the time between the two pulses, and this is converted to a position on a time histogram.[16]	23
4.4	Main window of LUNDtofs program while autotition is running	24

5.1	Comparing results of the rebuild system with reference data from [17]. Areas sampled are chosen due to the absorption features present, one for each detector range.	26
5.2	Comparing measurements taken on a 1.91mm BG36 sample, using a AOTF/NIR1 filter with the 6 W and 10 W lasers respectively.	26
5.3	Full Width, Half Maximum for the IRF signal using the AOTF, and the LLTF with different fibres	27
5.4	Comparing results from measures on a 1.91 mm thick BG36 sample, using the LLTF and AOTF filters. Data from [17] included as reference.	28
5.5	Comparing results from measures on a 3.64 mm thick BG36 sample, using the LLTF and AOTF filters. Note the higher absorption maxima for the LLTF and the larger dips in the scattering curve for the AOTF.	29
5.6	Comparing results from measures on a N18ln2c tablet sample, using the LLTF and AOTF filters. The absorption maxima can be seen to be higher for the LLTF, and there are larger dips in the scattering curve for the AOTF.	29
6.1	Optical fibres attached to the lower left arm of the test subject. .	31
6.2	Muscle tissue spectra measurements with 20 mm fibre separation. There is good correspondence between the absorption in (a) with the reference Arm(thinner) in (c) , except for the prominent water peak at 970 nm. The measured scattering in (b) is similar to the reference (d) . [12]	33
6.3	Absorption and reduced scattering spectra taken on arm muscle with 20 mm fibre separation, 960 - 1340 nm.	35
6.4	Comparing absorption and reduced scattering spectra recorded with 10 mm and 20 mm fibre separation, 650 - 1000 nm.	35
6.5	Two curve fits on the same data, where (a) is unmodified while (b) have a delay of 44 ps introduced for the IRF. The blue dotted curve is the measured data and the red curve is the computed theoretical model. For a good fit they should overlap. Notice the shift in the shaded IRF curve between (a) and (b) . Each channel represents 3 ps.	36
6.6	Comparing spectra taken with 10 mm and 20 mm fibre separation, 960 - 1340 nm.	37
6.7	Spectra for absorption and reduced scattering coefficients of muscle in lower arm, taken with 10 mm fibre separation. 650 nm - 1340 nm	39

Abbreviation

AOTF	Acusto-Optic Tunable Filter
FWHM	Full Width, Half Maximum
IRF	Instrument Response Function
MC	Monte Carlo simulation
NIR	Near Infrared
LLTF	Laser Line Tunable Filter
PMT	Photo Multiplier Tube
pTOFS	photon Time-of-Flight Spectroscopy
RTE	Radiative Transfer Equation
SPAD	Single photon avalanche photodiode
TCSPC	Time-Correlated Single Photon Counting
VIS	Visible
μ_a	Absorption coefficient
μ_s	Scattering coefficient
μ'_s	Reduced Scattering coefficient

1 Introduction

This chapter will present a short background for this work, followed by a presentation of the goals for the thesis. The chapter is concluded by describing the structure of the report.

1.1 Background

In many applications it can be useful to measure the absorption of light in a sample or object, even samples that scatter light a lot. One example is to measure the amount of oxygen in blood, where knowing the absorption at two different wavelengths will give a ratio between the haemoglobin carrying oxygen and that without oxygen. Another example is that the absorption spectrum may vary between tissue types, possibly enabling detection of tumours if the characteristics of both healthy tissue and tumours are known.

One method of doing this is with photon Time-of-Flight Spectroscopy (pTOFS), where the absorption and scattering values are computed from the shape of a histogram over the flight time for photons passing through a sample. The Biophotonics Group at the Department of Physics at Lund University have used a pTOFS system for measuring the properties of numerous substances, ranging from medical tablets to live human tissue.

1.2 Aim of the thesis

The object of this work was to upgrade the system with new components, a new laser and a new optical filter, in effect constructing two parallel systems where parts could be switched depending on the sample, and then use the new system to measure the optical properties of human muscle tissue in the near infrared region. Measurements with pTOFS have not been done with wavelengths above 1000 nm on human muscle tissue before, but such experiments will be presented in this thesis.

To ensure that measurements made using the new components give reliable results, they will be compared with results from the previous system on target samples with known optical properties. The same experimental setup will be used, including optical fibre pathway, attenuators and detectors.

After the new hardware have been installed it will be used to acquire a spectra of the absorption and scattering properties of human muscle tissue. Since the absorption of lipids and water are known to have peaks with high values in this region, we expect to need the sharper spectral resolution that the new LLTF filter is specified for, as well as the higher output power provided by both the new laser and filter.

1.3 Structure

We conclude the introduction chapter by commenting on the structure of the paper. The parts that are included are as follows:

- The *Time of Flight Spectroscopy* chapter, which is aimed at presenting a overview of the basic theory and components and how the measurements are carried out. More detailed theory and descriptions are given in separate chapters.
- The *Theory* chapter, presenting a more fundamental background of the theory.
- The *Instrumental setup* chapter, presents more details of the hardware components and of the software used for collecting and evaluating data.
- The *New system setup* chapter, describing the installation and evaluation of the new laser and optical filter.
- The *Muscle tissue measurements* chapter, where the work on recording the optical properties for muscle tissue is presented. The resulting spectra is also presented and discussed.
- The *Concluding remarks and Outlook* chapter, being the final part where concluding remarks and final thoughts are presented.

2 Time of Flight Spectroscopy

This chapter is intended to serve as a springboard for the rest of this thesis, so that the reader may have some basic understanding of the photon Time-of-Flight Spectroscopy (pTOFS), being the basis for this work. We will begin with a section introducing the concept of pTOFS and the optical theory behind it, then move on to a brief description of the optical components, followed by a section about data handling and a description of the two target geometries used for the measurements described in this thesis. The chapter is concluded with a summary of the measuring procedure.

More in depth theory can be found in chapter 3, while the components and instrumental set-up are described in detail in chapter 4.

2.1 Introduction

Absorption spectroscopy is an optical technique that has seen widespread use in modern society. Traditionally light is sent through a clear, but coloured object, then by measuring the absorbed light and comparing with known absorption spectra of different materials, the composition can be identified. Further, if the optical pathway is known the absolute concentration of the components can be calculated. In a clear target such as a glass of water this is relatively simple. The method is the standard practice for measuring concentrations in clear samples, used in innumerable applications all over the world. However, in turbid materials, such as for instance milk, this becomes significantly more difficult. As the white colour of milk comes from light being scattered many times as it travels, the amount and colour of the light passing through now depends not only on the absorption but also of the scattering properties of the material. These types of effects appear in many applications, including biological tissue and pharmaceutical tablets.

2.1.1 Absorption and scattering

The amount of absorption and scattering in the medium under study can be described by the absorption coefficient μ_a and the scattering coefficient μ_s , respectively. The absorption coefficient describes the probability that a photon is absorbed per unit pathlength travelled and is usually given in reverse centimetres [cm^{-1}], it equals the mean free path a photon on average travels before being absorbed. Higher absorption therefore means lower penetration depth into the media.

The scattering coefficient μ_s states the probability of scattering per unit pathlength travelled and is also given in [cm^{-1}]. Since often scattering is not completely random but have an angular probability the anisotropic coefficient g is introduced together with the reduced scattering coefficient $\mu'_s = \mu_s(1 - g)$. The mean path travelled by a collimated beam of light before it becomes effectively isotropic is given by $1/\mu'_s$.

2.1.2 Time of Flight Spectroscopy

The technique pTOFS was introduced as a method to obtain both μ_a and μ_s at the same time in a scattering media. The phenomena making pTOFS possible is that the path of different photons going through a scattering media is somewhat random and will thus be of different lengths, i.e. they exhibit different time-of-flights (TOF).

The photons may take different paths between the source and the detector, while some of the paths are more likely than others. Photons travelling close to a surface run a high risk of being scattered out of the media, while photons travelling deep into the media have a higher accumulated risk of being absorbed. A pulse passing through will therefore be broadened according to the statistical distribution of passing photons as illustrated in Figure 2.1.

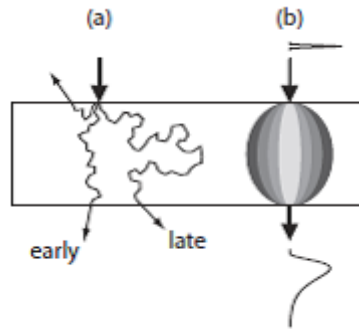


Figure 2.1: Part (a) shows different paths a photon can take. The time it takes for a photon to pass depends on the path. Those travelling relatively straight with few scattering events, will arrive earlier than those that scatter many times. Late photons will have a larger probability of being absorbed, as the absorption depends on the path length travelled. Some photons will be lost as they exit through the tissue boundary. Part (b) shows the statistical distribution for the photons and how the light pulse is broadened in time. [1]

By sending many short light pulses into the sample and detecting the time it takes for photons to reach a detector at some distance away, we can get a time resolved distribution curve where time corresponds to pathlength of the detected photon. The shape of the curve is determined by the values of μ_a and μ_s , and by fitting a model curve to the experimentally measured curve, we can extract those values. In essence we use a theoretical model and guess initial values of μ_a and μ_s to create a curve, which is compared to the experimental one. If the curve doesn't fit then we change the values a little and compare again, repeat this process until an acceptable curve fit is found. The absorption and scattering values of the final curve is then taken to represent the experimental curve.

To improve the performance of the parameter determination we introduce a couple of extra measures in addition to sending light pulse through the sample. The theoretical simulations used all assume that the light pulse is infinitely short. Since the pulse from the laser used in the measurements is not negligibly narrow and will be even further dispersed from passing the optical components,

we need to feed the pulse width into the fitting procedure somehow. This is done by recording a time curve with the exact same setup but with a piece of black paper as the sample. We call such a measured curve the *Instrument Response Function* (IRF), and the theoretically modelled pulse is then convoluted with the IRF to produce a curve for fitting the experimental data.

The time resolution of the system has to be very fine to differentiate the pathlength of individual photons, so the components used also have to be very precise. Unfortunately some parts exhibits a temporal drift over time, which means the IRF and the sample pulse peaks might not be recorded at the same relative time position. This is remedied by splitting off a small part of the laser pulse and sending it directly to the detector without passing through the sample. This measured peak is called the *time reference pulse*. Since this pulse experience no broadening from sample scattering, it is easy to correlate pulses from the IRF and experimental data. The peaks of the time reference should be at the exact same position as the sample, if not then the IRF will be shifted so that they overlap (Figure 2.2).

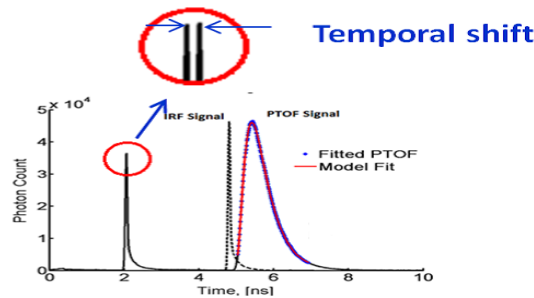


Figure 2.2: The measured data and the time reference can be seen in the result of a model fit. The sharp peaks at 2 ns are the time reference pulse used to correct for any temporal shift. They should overlap, if they do not then the IRF data is shifted. Modified from [2]

Another complication is the fact that the pulses are not only the exact wavelength we want, but rather a Gaussian curve with a width of 3 - 12 nm around this wavelength, the width depending on the filter and wavelength range. Not only does this limit the resolution of our measurement, but close to absorption peaks of the material it influences the accuracy of the fitting and also affects the computed scattering. The varying absorption creates a distortion of the shape of the detected pulse [2], and this is translated into lower scattering by the theoretical modelling. These cross talk dips in the scattering curve are usually easy to recognise, as the scattering generally decreases monotonically with wavelength, but might coincide with actual features of the sample making the results harder to interpret.

The cross talk from absorption to scattering is greatly affected by the spectral width of the filtered light, so the optical filters should preferably deliver as spectrally narrow shape as possible.

2.2 Instrumental setup

The main components of the pTOFS system can be seen in figure 2.3. Short light pulses are created with a supercontinuum laser source that provides light from 450 nm to 1800 nm. The light is fed into an adjustable optical filter that lets us select a small part of the light spectrum to be used in the measurements. The output of the filter is connected to a beam splitter that diverts a small fraction of the light pulse to be used as time reference, the remainder is passed through to the sample via a gradient index fibre. The scattered light pulse is collected with another optical fibre, and then both the time reference and the sample pulse are combined in a beam recombiner and sent to a detector. When the detector registers a photon it sends a pulse to the counting card on the computer, the time relative to a synchronizing pulse from the laser is recorded and collected into a time distribution curve.

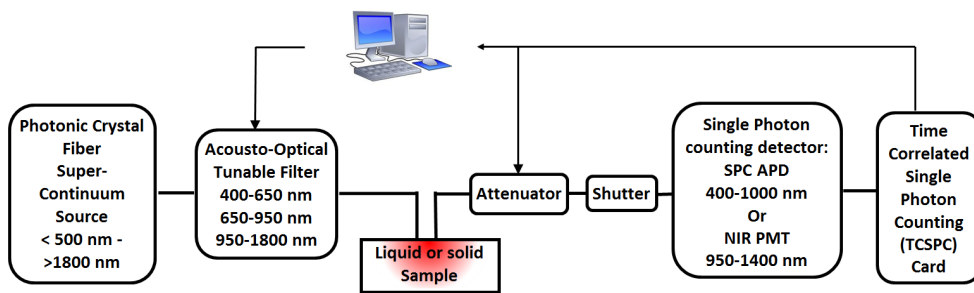


Figure 2.3: Schematic arrangement of the pTOF spectrometer [3]

Since the detector will only register the first photon to arrive, it is important that the chance of a photon passing the media into the detector fibre is low so the odds for two photons passing can be neglected. We attain this by placing variable attenuators in the optical path so that only a fraction of the light will be detected. The count rate of detected photons per second is used as a measure for the probability of the chance for photons to pass, if we detect too many photons then the attenuation can be increased. On the other hand we want a high count rate to get more statistically accurate results, which limits how low count rate we can accept. In this thesis work we aim to stay at the same count rate in all measurements, approximately 10^5 counts/second, and adjust the attenuators accordingly for each measurement.

2.2.1 Lasers

Two different lasers by the same manufacturer are used during the experimental work, Fianium SC-480-10 and SC-500-6, providing 10 or 6W respectively over the whole bandwidth with a 80 MHz repetition rate. The SC-480-10 was completely new and installed as part of this project while the 6W SC-500-6 is part of an existing set-up.

2.2.2 Filters

Three different filters give access to tuned wavelengths across the laser output, all three provided by Fianium. Two are Acusto-Optical Tunable Filters (AOTF), each with two overlapping spectral settings. The first have output for visible light (VIS) in the range of 400 nm to 690 nm and near infra-red (NIR1) 650 nm to 1000 nm, the second have the same NIR1 range and further into infra-red (NIR2) at 950 nm to 1400 nm.

The third filter is a Laser Line Tunable Filter (LLTF) with a tunable wavelength reach of 1000 nm to 1800 nm. Like the 10 W laser it is a new component and was installed and evaluated as part of this thesis.

2.2.3 Detectors

Depending on what part of the spectra we measure in, two different detectors are used. For the region up to 1000 nm a single photon avalanche photodiode (SPAD) detector from MICRO Photon Devices is used, and between 950 nm and 1400 nm a Photo Multiplier Tube (PMT) from Hamamatsu Photonics.

2.3 Data handling

Control of the filters and attenuators are maintained with the help of a program named LUNDtofs, developed for the Biophotonics group at Lund University. LUNDtofs also receives data from the detectors via a controlling card installed on the computer, and stores it in files that can later be used for evaluation.

The collected data histograms are processed with help of a Matlab-program called "TimeResolved v3" that has been developed by the Biophotonics group at Lund University. The program sums up the collected data and let you choose different types of modelling to be carried out for guessing μ_a and μ_s , then implements a Levenberg-Marquardt algorithm in Matlab to fit the curves. The models used in evaluating the results for this thesis are *Diffusion Theory* and *Monte Carlo simulation*.

2.3.1 Diffusion theory

Diffusion theory is a popular and widely used model of light transport in turbid media. It is derived from simplifications of the *Radiative Transport Equation* (RTE), which mathematically model the transfer of energy as photons move inside a tissue. The diffusion theory is only valid under certain circumstances, the light propagating is diffuse, meaning that μ_s is much larger than μ_a and the distance between source and detector is large enough so that the light has become diffuse. The advantage of the diffusion model is that it is easy to calculate numerically.

2.3.2 Monte Carlo simulations

Monte Carlo (MC) uses another approach to simulate light transport in the turbid sample investigated. Also implementing the RTE it uses probability distributions, simulating the path of a package of photons by random walk steps. At each step the photon can be scattered or absorbed randomly according to the absorption and scattering probability values, until the package exits the sample

or is absorbed. By doing this a very large number of times and recording the end state for each photon, a statistical distribution of the light propagation can be derived. MC simulations gives accurate results regardless of the scattering and absorption values but is computationally heavy and therefore takes long time. If the detector and source are located far apart there can be a problem acquiring good statistics as a very large number of simulations need to be performed to get high count of photons that exit at the simulated detector point.

2.4 Target setup

In the work for this thesis there are two types of measurements performed, either on tablets fixed in a holder or on live muscle tissue with optical fibres positioned against the skin.

2.4.1 Tablet measurements

To test the performance of the LLTF filter and validate that the optical components were assembled in a correct way, several measurements were recorded on reference tablets and the results were compared to previous data. The tablets are fixed inside a hollow tube, with connections for optical fibres at each end (Figure 2.4). The set-up insures that the fibres are aligned properly and keeps the fibre tips and the sample from coming in direct contact, lowering the chance of damage or contamination to either.

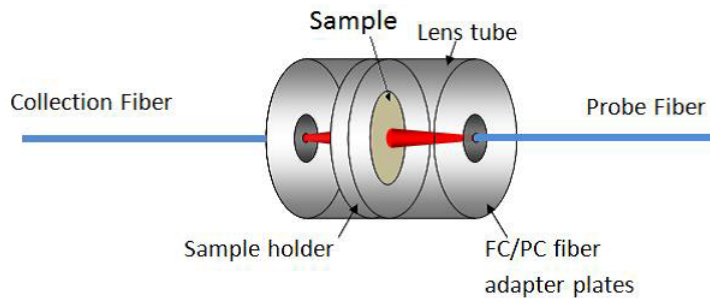


Figure 2.4: Sketch of the tablet holders, modified from [2]

The tablets that are used for reference, and also for comparison between the filters, consist of powder from a crushed Shott BG36 color filter combined with titanium oxide in an epoxy resin base [2].

A second comparison between the filters are done with medical tablet samples marked N18ln2C. The IRF measurements are recorded using a piece of double printed black paper fixed in a holder of the same type.

2.4.2 Muscle measurements

The muscle tissue experiments are done by fixing two optical fibres in a plastic holder, shown in Figure 2.5, that is then positioned and fixed against the left forearm of the subject. The forearm is used due to the relatively thin skin

layers, and the fibre holder position is chosen with regards to blood vessels and tendons so that the sample area consists mainly of muscle tissue.

The IRF measurements are made by positioning the two fibres opposite each other in a holder with a piece of double printed black paper in between. The paper is changed for each new series of measurements due to the possibility of the fibres scratching the black print.



Figure 2.5: Fibre holder with the two optical fibres

2.5 Measuring procedure

The typical measure procedure is as follows: If the PMT detector is to be used, the first thing done is to start the cooling, as it needs time to get a stable temperature control. Next the laser used is started, but with zero light output, so that the laser power source has time to stabilize. The optical path of the system is checked, i.e. coupling the optical fibres to the desired combination of filter, sample holder and detector. The controlling computer is connected to the components, including laser reference to the counting card, filter control and detector signal. The LUNDtofs program is started on the computer, initializing the attenuators, the data collecting and the filter controls. The attenuators are set at maximum attenuation, -40 dB, to help minimize the danger from any light leakage.

Next the output fibre from the filter is connected to a spectrometer via an attenuator, and the laser is put into operational mode. The fibre coupling to the filter is fine-tuned to maximize the output intensity, with the help of adjusting screws on the coupling. Laser output is then blocked, either on the laser or with shutters mounted on the filters, the spectrometer is removed and the main experimental setup is rebuilt. The reason to building the setup first, then do fibre tuning only to recouple the fibre to the system again is to reduce the need to change fibre connections. Even with the laser output blocked there is always a small risk of leakage, so the instances any fibre is unconnected should be minimized.

2.5.1 Measurements

Two sets of measurements are made for each wavelength, one for the sample and one IRF (Instrument Response Function). The sample is usually measured first, as the count rate for the IRF needs to be lower than the sample due to peak broadening in the data evaluation, thus we need to know the count rates from the sample as they vary greatly with wavelength.

Each measurement is done by collecting one data sample every second for 25 seconds. The attenuators are adjusted before the measurement to get as close to $10 \cdot 10^4$ counts/second as possible for a sample, or $9 \cdot 10^4$ counts for IRF, and the measure cycle is started in the LUNDtofs program. The result is saved to a file with a name corresponding to the wavelength and sample name or IRF. The wavelength is then changed according to the step size desired for the measurements, and the procedure is repeated. At the start of the work for this thesis the measurements were made manually, but as work progressed on implementing the filter drivers with the LUNDtofs program, later measurements are made semi-automated. Since the IRF count rate needs to be lower than the sample, the system could not run on it's own when the counts have to be recorded. The IRFs where then made manually when the counts where not at $10 \cdot 10^4$ per second in the automated cycle.

When both sample and IRF measurements are finished, the saved data is imported into the Timeresolved Matlab program for processing and curve fitting. The resulting values of the absorption and scattering coefficients is then plotted and evaluated.

3 Theory

This part is aimed at providing the knowledge and formalism needed in order to understand and treat the problem at hand.

3.1 Light propagation in turbid media

The theory of light propagating in turbid media could be seen as relying heavily on treating light as particles, while both diffusion and Monte Carlo are ways to solve the RTE, thus not limiting the picture to light as a stream of particles. However, often in the field of biomedical optics the discussion often are expressed a bit naive in terms of transport of light particles. Being aware of this distinction, we will here follow the normal practice with a naive picture of light as photons travelling in straight paths. Occasionally, a photon interacts with a material particle and change direction or is absorbed. The only time wave optics come in play is to determine the effects of such encounters, such as defining the scattering coefficient μ_s and the scattering phase function $p(\hat{\mathbf{s}}, \hat{\mathbf{s}}')$. [4]

3.1.1 Absorption

The absorption of light is determined by the Beer-Lambert law:

$$I = I_0 \cdot \exp(-\mu_a \cdot L) \quad (3.1)$$

where I is the intensity of light transmitted through the media, I_0 is the initial light intensity and L is path length travelled. The absorption coefficient μ_a [cm^{-1}] expresses the probability of the photon to be absorbed per unit path length. If the energy of the photon matches the distance between two energy levels in an atom or molecule, then the photon energy can be transferred to the atom and the photon is annihilated. Since the energy levels of atoms and molecules are unique, the absorption spectra can be used for identification. The inverse of μ_a is the average path length travelled before absorption.

3.1.2 Scattering

In turbid media the scattering effect is much higher than the absorption, meaning that light propagation is mainly influenced by the scattering coefficient μ_s [cm^{-1}]. This gives the probability of an scattering occurring per unit path length. There are two types of scattering; elastic and inelastic. Elastic scattering means the photon have the same energy after the event as it had before, and inelastic that the photon energy changes.

Elastic scattering can be of two types, Rayleigh or Mie. Rayleigh is an approximation of Mie scattering that is valid only when particle size is much smaller than the incident wavelength, while Mie holds for any spherical particle of a size comparable to the wavelength. Rayleigh follows a λ^{-4} dependence for the scattering cross section, while Mie follows $a \cdot \lambda^b$, where a and b are constants with b smaller than 4. Mie scattering can be used to explain why the clouds are white (larger water droplets), but the sky is blue due to Rayleigh scattering

(small air molecules).

Raman scattering is an process where part of the photon energy is transferred to the scattering molecule, in tissue it is very weak effect that for the most part can be ignored.[4]

3.1.3 Scattering phase function

The direction a photon is scattered into is determined by the scattering phase function $p(\hat{\mathbf{s}}, \hat{\mathbf{s}}')$, describing the probability of scattering from direction $\hat{\mathbf{s}}$ to direction $\hat{\mathbf{s}}'$. A frequently used phase function is the Henyey-Greenstein phase function

$$p(\cos\theta) = \frac{1 - g^2}{2(1 + g^2 - 2\cos\theta)^{3/2}} \quad (3.2)$$

where θ is the inclination angle between the two directions. g represents the tendency towards forward scattering and is called *anisotropy factor* or simply "g-factor", it is defined as $g = \langle \cos\theta \rangle$. Completely isotropic scattering would have $g = 0$ while values of g close to 1 represents heavy forward scattering, Figure 3.1. Taking the angular tendency into account for the scattering leads us to the *reduced scattering coefficient* μ'_s [cm^{-1}], defined as

$$\mu'_s = (1 - g)\mu_s \quad (3.3)$$

The reciprocal of μ'_s states how often, on average, light undergoes a complete change in propagation direction. [1, 5]

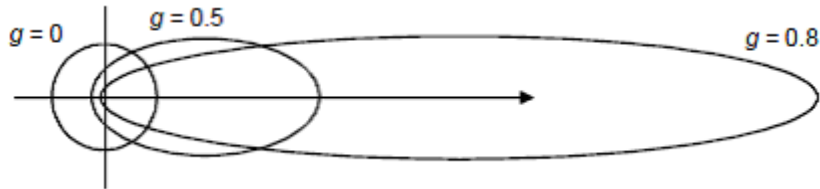


Figure 3.1: The Henyey-Greenstein phase function for different values of the scattering anisotropy g-factor. [5]

3.2 Radiative Transfer Equation

The radiative transport theory considers light to be a number of independently moving particles that do not interact with each other, expressing the energy balance inside a given volume with regards to conservation of energy. When a photon is absorbed all the energy is considered to be transferred to heat, all scattering events assumes the photon change direction but the energy is unchanged.

Now lets consider a small volume V with the surface area A . The number of photons travelling in the direction $\hat{\mathbf{s}}$ inside the volume can change in four ways, shown in Figure 3.2.

- a) radiance through the boundaries A
- b) photons absorbed or scattered into another direction
- c) photons scattered from another direction to the direction of $\hat{\mathbf{s}}$
- d) photons added by sources inside the volume V

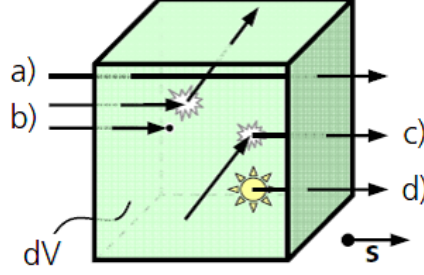


Figure 3.2: Terms included in the RTE; (a) radiance, (b) losses due to absorption or scattering, (c) gains from scattering, (d) sources. [6]

The boundary term a) represents photons passing in or out of the volume V through the surface boundary A , with the speed of light of the material c . If number of photons at a position $\bar{\mathbf{r}}$ is expressed as $N = N(\bar{\mathbf{r}}, \hat{\mathbf{s}}, t)$ then the boundary transfer is

$$\left(\frac{\partial N}{\partial t}\right)_{transfer}^V = - \int_A cN \hat{\mathbf{s}} \cdot \hat{\mathbf{n}} dA = - \int_V c \nabla N \cdot \hat{\mathbf{s}} dV \quad (3.4)$$

The second term consists of losses from absorption and scattering. The absorption at a position $\bar{\mathbf{r}}$ is given by $\mu_a(\bar{\mathbf{r}})$ and the probability of a photon being absorbed during a short time dt is $\mu_a c dt$, so the photons lost to absorption are

$$\left(\frac{\partial N}{\partial t}\right)_a^V = - \int_V c \mu_a(\bar{\mathbf{r}}) N dV \quad (3.5)$$

The losses due to scattering can in the same way be described by

$$\left(\frac{\partial N}{\partial t}\right)_{s-}^V = - \int_V c \mu_s(\bar{\mathbf{r}}) N dV \quad (3.6)$$

Photons that were travelling direction $\hat{\mathbf{s}}'$ but are scattered into $\hat{\mathbf{s}}$ are expressed in term c) and depends on the scattering μ_s and the phase function $p(\hat{\mathbf{s}}, \hat{\mathbf{s}}')$

$$\left(\frac{\partial N}{\partial t}\right)_{s+}^V = \int_V c \mu_s(\bar{\mathbf{r}}) \int_{4\pi} p(\hat{\mathbf{s}}, \hat{\mathbf{s}}') N(\hat{\mathbf{s}}') d\omega' dV \quad (3.7)$$

If a source of light exists inside the volume then the gain of photons is described with the help of a source function $q(\bar{\mathbf{r}}, \hat{\mathbf{s}}, t)$

$$\left(\frac{\partial N}{\partial t}\right)_{source}^V = \int_V q(\bar{\mathbf{r}}, \hat{\mathbf{s}}, t) dV \quad (3.8)$$

Since the volume is arbitrary we can drop the integrals and combine the elements into the *Radiative Transfer Equation* (RTE) [1]

$$\frac{\partial N}{\partial t} = -c\nabla N \cdot \hat{\mathbf{s}} - c(\mu_a + \mu_s)N + c\mu_s \int_{4\pi} p(\hat{\mathbf{s}}, \hat{\mathbf{s}}')N(\hat{\mathbf{s}}')d\omega' + q \quad (3.9)$$

3.3 Diffusion model

It is not possible to solve the RTE analytically in a 3D environment, and numerical solutions require long computational times, but under certain circumstances the RTE can be reduced to a diffusion model. One of the most used methods is by expansion of spherical harmonics. [7]

We can describe the radiance L by it's relation to N as

$$L(\bar{\mathbf{r}}, \hat{\mathbf{s}}, t) = N(\bar{\mathbf{r}}, \hat{\mathbf{s}}, t)hc\nu \quad (3.10)$$

where h is the Plank constant and ν is the frequency of the light. By expanding L into spherical harmonics Y_{lm} and truncating the expansion at the first order, we get [6]

$$\begin{aligned} L(\bar{\mathbf{r}}, \hat{\mathbf{s}}, t) &= \sum_{l=0}^{\infty} \sum_{m=-1}^l \sqrt{\frac{2l+1}{4\pi}} L_{lm}(\bar{\mathbf{r}}, t) Y_{lm}(\hat{\mathbf{s}}) \\ &\approx \frac{1}{4\pi} (\phi(\bar{\mathbf{r}}, t) + 3\mathbf{F}(\bar{\mathbf{r}}, t) \cdot \hat{\mathbf{s}}) \end{aligned} \quad (3.11)$$

The interpretation of Eq. (3.11) is that the radiance has been divided into an isotropic term, the *fluence rate* ϕ , and one term describing the angular dependence, the *flux* \mathbf{F} , while higher order terms were neglected. We also assume that the source is isotropic:

$$q(\bar{\mathbf{r}}, \hat{\mathbf{s}}, t) = \frac{1}{4\pi} q_0(\bar{\mathbf{r}}, t) \quad (3.12)$$

Inserting Eq. (3.11) and (3.12) into the RTE (Eq. (3.9)) and integrating over the full 4π solid angel, we obtain the following scalar equation;

$$\frac{1}{c} \frac{\partial \Phi(\bar{\mathbf{r}}, t)}{\partial t} + \mu_a \Phi(\bar{\mathbf{r}}, t) + \nabla \mathbf{F}(\bar{\mathbf{r}}, t) = q_0(\bar{\mathbf{r}}, t) \quad (3.13)$$

and by multiplying with $\hat{\mathbf{s}}$ before integrating we get;

$$\frac{1}{c} \frac{\partial \mathbf{F}(\bar{\mathbf{r}}, t)}{\partial t} + (\mu_a + \mu'_s) \mathbf{F}(\bar{\mathbf{r}}, t) + \frac{1}{3} \nabla \Phi(\bar{\mathbf{r}}, t) = 0 \quad (3.14)$$

Assuming that the temporal change in flux is negligible, i.e. $\partial \mathbf{F} / \partial t = 0$, Eq (3.14) reduces to Fick's law

$$\mathbf{F}(\bar{\mathbf{r}}, t) = -D \nabla \Phi(\bar{\mathbf{r}}, t) \quad (3.15)$$

with the *diffusion coefficient* D defined as

$$D = \frac{1}{3(\mu_a + \mu'_s)} \quad (3.16)$$

By inserting Fick's law (Eq. (3.15)) into Eq. (3.13) and assuming that we have a homogeneous media where D is constant we arrive in the *Diffusion Equation* (DE)

$$\frac{1}{c} \frac{\partial \Phi(\bar{\mathbf{r}}, t)}{\partial t} = D \nabla^2 \Phi(\bar{\mathbf{r}}, t) - \mu_a \Phi(\bar{\mathbf{r}}, t) + q_0(\bar{\mathbf{r}}, t) \quad (3.17)$$

The Diffusion Equation is only valid if the light is diffuse, which implies scattered many times and thus that the scattering is much higher than absorption, i.e. $\mu'_s \gg \mu_a$. The fluence Φ must also be calculated far enough away from the source to allow the light to become diffuse.

3.4 Monte Carlo

While diffusion theory is fast and convenient to model light transport, it is not usable when absorption is not weak compared to scattering, or close to sources. Here Monte Carlo (MC) simulations can be applied instead.

Monte Carlo simulation uses probability distributions to model propagation of light. Because the physics of elastic light scattering and absorption processes is relatively simple, the model is not too difficult to implement. The required parameters for a MC simulation are the scattering coefficient, the absorption coefficient and the scattering phase function.

Based on the transport equation, MC treats photons as particles and neglects all wave properties. Each photon or packet of photons is traced through the media by random walk, the distance travelled in each step is randomly determined based on the scattering and absorption coefficients. At the end of each step, the weight of the photon packet is reduced by absorption, the remainder is then redirected in a random direction according to the phase function. Once the new trajectory is decided, the photon packet again move a random distance, and so on, until the photons either exit a media boundary or is absorbed. If this method is applied repeatedly for a large numbers of particles, the traces for these particles may be used to estimate how the entire population behaves in the medium. [4]

The drawback of Monte Carlo is that it is computational heavy. A great many simulations need to be run to get a statistically significant result, and an increase in distance between the source and the detector means more simulations are required. For this thesis work we used a database of simulations that had been compiled previously by the Biophotonics group, specified for tissue in a semi-infinite geometry.

3.5 Resolution effects

For best results the laser pulse should be infinity narrow in spectral resolution, a sharp peak at exactly the desired wavelength. However this is not possible to achieve with the equipment we use, instead the pulse is an Gaussian curve with a width of 3 - 12 nm depending on wavelength.[8]

This means that the measured optical properties is a convolution of the Gaussian spectrum and the absorption values. Where the absorption vary only slightly with wavelength this is not a issue, since then the measured value will be close to the real one, but if the absorption changes rapidly then the recorded distribution will be distorted. For instance, with a sharp rise in μ_a the higher wavelengths will be absorbed more, and the lower ones less, than the centre that is the actual target. This will generally result in a lower evaluated absorption coefficient. The resulting histogram will also be interpreted by the modelling software as having lower scattering, this can be seen as dips in the otherwise monotonically decreasing scattering curve.

3.6 Biological tissue

Most biological tissue are highly scattering, and in the 400 to 1350 nm spectral region the absorption is usually weaker so the light can be regarded as diffuse after a short distance through the tissue. The region from 600 to 1000 nm have particularly low absorption, making this a prime range for optical measurements, and is referred to as the tissue optical window [7]

Optical absorption in this region originates from haemoglobin, melanin and water. Haemoglobin exhibits two forms, oxygenated and deoxygenated. Figure 3.3 shows the absorption spectra of these primary absorbers.

Absorption in the ultraviolet region is usually very high, so the optical penetration is much shorter in this region which makes it less interesting for turbid material spectroscopy.

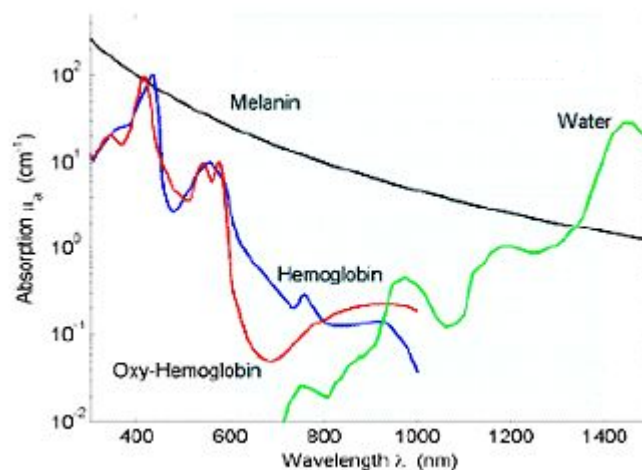


Figure 3.3: Tissue optical window. Modified from [9]

There are a couple other chromophores that affect measures mainly above 900 nm. Collagen and elastin make up a small part of muscle tissue and have an absorption peak at 1180 nm. Lipids are present in for instance the subdermis and is characterized by three absorption peaks around 920, 1040, and 1210 nm (Figure 3.4).

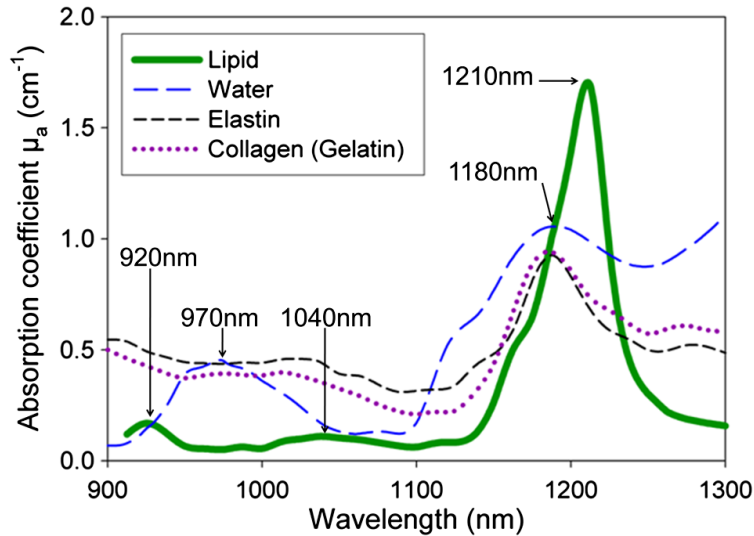


Figure 3.4: Absorption coefficient spectra of lipid, water, elastin, and collagen. [10]

3.6.1 Muscle tissue

Muscle tissue is made up from individual components know as muscle fibre, consisting of long cylinders of about 1-2 μm diameter called myofibrils. What we generally call a muscle is a collection of such fibres held together in bundles by a supporting tissue, which also serves as a pathway for nerves and blood flow into the muscle.

The main absorbers in muscle tissue are water and haemoglobin. The optical properties have been measured previously by many groups, one such set of measurements can be found in table 3.1. The absorption is high at 633 nm originating from the haemoglobin content, at longer wavelengths the effect of water absorption dominates [11].

3.6.2 In vivo measurements

The measurements for this thesis use optical probes placed on the surface of the skin. Since the skin and the subcutaneous fat layer lies between the fibres and the muscle, the result is not from muscle tissue alone, in particular the lipids in the subcutaneous fat affects the measurements as is shown in Figure 3.5. The fat layer does not contain much blood or water so their high absorption peaks are masked by the lipids. To minimize this effect as much as possible the forearm was chosen for the measurements due to the fact that the subcutaneous

λ, nm	μ_a, cm^{-1}	μ'_s, cm^{-1}
633	1,23	8,94
700	0,48	8,18
750	0,41	7,71
800	0,28	7,04
850	0,3	6,67
900	0,32	6,21
950	0,46	5,9
1000	0,51	5,73

Table 3.1: Absorption and scattering values for muscle tissue, data from [11].

fat layer is relatively thin there.[12]

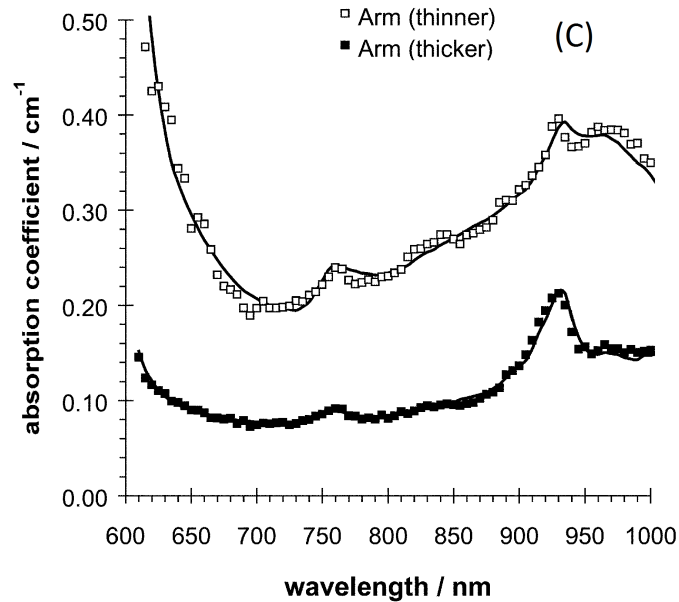


Figure 3.5: Absorption spectra from forearm of two subjects with different fat layers. The muscle tissue properties are masked by the lipids in the skin, as the light will not penetrate deep enough [12].

The statistically most probable path of the photons is shaped like a banana, with a maximum depth of half the probe distance [18], this means that with larger separation of the fibres the main body of the detected photons will travel more deeply into the tissue. The distance between fibres therefore decides what part of the tissue we are measuring, by selecting proper distances we can have the main path through muscle tissue and minimize the effects of skin and subcutaneous fat. Care have to be taken to avoid underlying structures though, as the arm is run through by several large blood vessels and tendons, both of which will have an effect on the measured data.

4 Instrumental setup

A sketch of the system setup can be found in Figure 4.1 and a more detailed schematic is given in appendix A. Briefly a supercontinuum laser source provides a spectrally broad pulse. The pulse is led to a tunable optic filter, where a narrow pulse of the desired wavelength is obtained. The light is led by an optical fibre to a beam splitter, diverting a small part as the time reference pulse. The main pulse is then lead to the sample and collected again after passing through, resulting in a broadened pulse. The sample and time reference pulses are combined again and led to a detector, the output of which is connected to a TCSPC counting card in a computer.

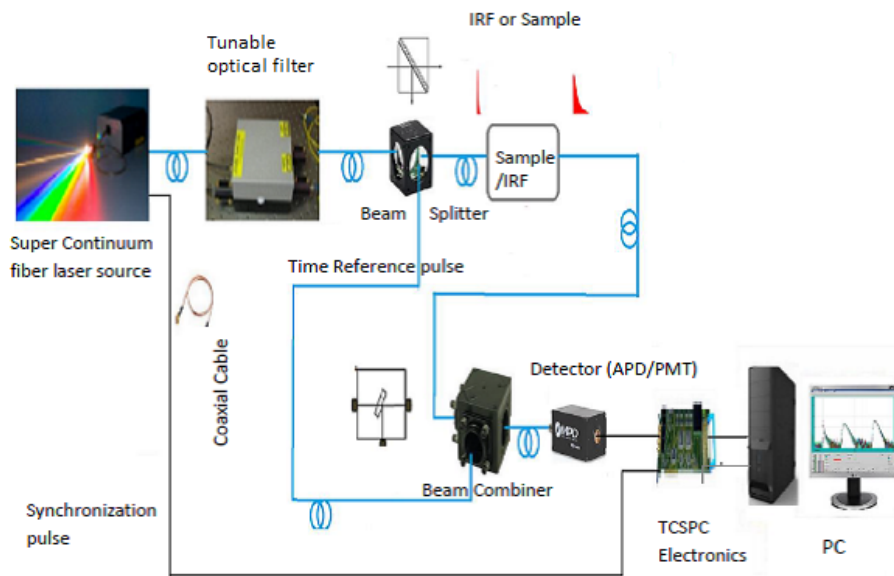


Figure 4.1: The setup of the Photon Time of Flight system. A broadband laser is connected to a filter that is tunable to only let a selected wavelength pass. The pulse is then split into an Instrumental Response Function (IRF) and a Sample arm. After the light have passed the sample the two pulses are recombined and led to a single photon counting detector. A counting card record a histogram that is then sent to a controlling software program. Modified from [13].

4.1 Lasers

Two different laser are used, Fianium SC-480-10 and SC-500-6, providing 10 or 6 W total output respectively. The 10 W laser is new while the 6 W source is part of an existing experimental setup. Both are super-continuum sources. The advantage of using a super-continuum source is that one can select any desired wavelength out of the broad spectrum with the help of filters.

The lasers used consists of three main sub-systems: a master source, a high power amplifier and a non-linear super-continuum generator, shown in Figure

4.2. The master source is a passively mode locked fibre laser based on a core-pumped, Yb-doped fibre. It has a repetition rate of 80 MHz with a fundamental pulsewidth of 6.0 ps.

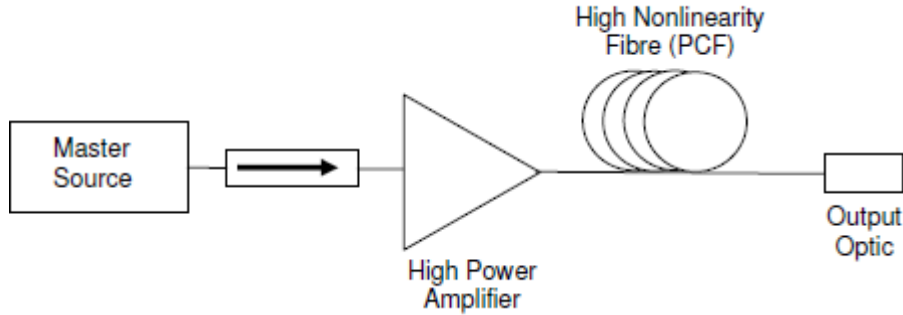


Figure 4.2: Functional diagram of a supercontinuum fibre laser source. A Master fibre laser creates a light pulse of a fixed wavelength, that is amplified and sent to a Non-linear fibre where it is spectrally broadened. [8]

The source is coupled to an amplifier, a Yb-doped fibre with double cladding, pumped by a high power laser diode pump module. With higher amplification rates both the optical output power and the spectral bandwidth are increased. A broad spectrum is then generated in a super-continuum generator which consists of a highly-non-linear optical fibre. The high pulse power together with the non-linearity results in a broadened spectral range from 450 to 1750 nm for the 6 W SC-500-6 laser, while the 10 W SC-480-10 can deliver light from 450 nm up to 2400 nm.

4.2 Filters

Three different filters are used to provide the desired wavelength. Two are Acusto-Optical Tunable Filters (AOTF), the third filter is a Laser Line Tunable Filter (LLTF). Both types of filters can be controlled through a computer

4.2.1 AOTF

The Acusto-Optical Tunable Filters consists of birefringent crystals, which changes the refractive index when exposed to an acoustic wave. The wave is created by alternating electric voltage over a piezoelectric crystal, resulting in a standing wave pattern where the refractive index changes due to the acoustic pressure. This creates a grating in the crystal which scatters the light depending on the wavelength. By choosing the correct vibration frequency, light of the desired wavelength is focused on a opening where it is collected and transmitted to an optical fibre.

The two filters used are Fianium AOTF-DUAL system, each housing two crystals with different wavelength regions. One is equipped with VIS/NIR1 crystals while the second houses NIR1/NIR2 ones, see table 4.1 for specifications.

<i>AOTF crystal</i>	<i>VIS</i>	<i>NIR1</i>	<i>NIR2</i>
Wavelength Range	400 to 700 nm	650 to 1100 nm	1050 to 2000 nm
Channel Bandwidth	2 - 4 nm	3 - 6 nm	6 - 12 nm

Table 4.1: AOTF specifications [8]

4.2.2 LLTF

The Laser Line Tunable Filter is based on the Bragg Tunable Filter technology. It consist of a volume hologram where the refractive index varies periodically. Only a narrow band of light will interfere constructively with the refractive index modulation and satisfy the Bragg condition, all other wavelengths will continue unaffected. By changing the angle to the incoming light the filter can be tuned over several hundred of nanometres. The volume hologram leads to a divergent beam, but by letting it pass a second time it is possible to recombine the beam and compensate for this [14].

The filter used for this thesis work is a Fianium LLTF Contrast SWIR with a spectral range from 950 to 2300 nm, with a spectral bandwidth of less than 5nm.

4.3 Fibres

Since the Time-of-Flight System measurements measures differences in time in the picoseconds scale, it is critical to minimize temporal broadening. One such area is the fibres transporting the light between the components. When light comes into an ordinary optical fiber with different angles, it travel with different speeds due to longer paths for light with higher angels, and the detected signal will be temporally broadened.

To avoid this GRIN fibres from Leoni Fiber Optics GmbH are used. The core fibre diameter is 400 μm (cladding diameter- 600 μm) which matches to the aperture of the smallest detector. GRIN fibre core has a refractive index that decreases with increasing radial distance from the fibre axis, so the velocity of the light is slower at the middle and gradually increases towards the edges.

4.4 Attenuators

Since the detector will only register the first photon to arrive, the chance of photons passing need to be low. To keep the rate at a constant level, two variable attenuators are positioned in the system. One is in the time reference pathway and the second is for the sample path. They also help protect the detectors from being overloaded with to high intensity of light. The attenuators are made by OZ Optics LTD, and have a remotely controlled variable attenuation from -2.6 dB to -40 dB.

4.5 Detectors

After combining the PTOF signal pulse and timing reference pulse in a optical combiner, they are sent to a single photon counting detector. Two detectors are used, depending on what wavelength region we have set the filters to.

4.5.1 SPAD detector (400 - 1000 nm)

A single-photon avalanche photo diode (SPAD) detector called PDM100ct from Micro photon Device is used for wavelengths shorter than 1000 nm. It has a photon detection efficiency of 49% at 550 nm and generate a TTL output pulse per detected photon [15].

4.5.2 PMT detector (950 - 1400 nm)

The second detector is a Micro-Channel Plate Photo Multiplier Tube (MCP-PMT) with InP/InGaAsP photocathode (R3809U-68 from Hamamatsu Photonics). Since it is susceptible to thermal noise it needs to be cooled down to -80°C , this also enhances the spectral range and sensitivity. The PMT can be damaged if the light level gets too high, therefore an automatic shutter is installed as protection.

Cooling is done with liquid nitrogen. The nitrogen is contained in a sealed dewar, with one outlet allowing liquid from the bottom to pass through the detector and a second outlet at the top, letting evaporated nitrogen escape to reduce pressure when a valve is opened. The valve is controlled by a Photocool series cooling unit from Research Inc. With the valve closed, pressure in the dewar rises as the liquid nitrogen evaporates, the pressure then push liquid through the bottom outlet, and is led to the detector to cool it. When the desired temperature is reached, the valve is opened and the pressure in the dewar drops to ambient room pressure, stopping the flow of liquid nitrogen to the detector.

4.6 TCSPC

Time-correlated single photon counting (TCSPC) is a very efficient technique for detection of individual photons with a high time resolution. It measures the time delay between two events e.g. between a photon arriving at a detector and a reference signal. At the start event a capacitor bank starts to charge at a constant rate, at the stop event it halts. By measuring the voltage after the stop, the time between start and stop can be calculated since the charge rate is known. By repeating the same measurement several times a statistical distribution of time delay is achieved as illustrated in Figure 4.3 (a).

The TCSPC module used is a SPC-130-EM from Becker & Hickl GmbH, the setup is shown in Figure 4.3 (b). It is set in reversed start-stop mode, meaning that when a photon is detected the clock starts, and stops at the next reference pulse from the laser. This setup is chosen because the TCSPC module needs a small amount of time to reset, and if reference pulse from the laser was used as start then early photons might not be detected. Another benefit is that now the detector only has to work when a photon is detected and not for every laser pulse.

4.7 Software

A computer is used to control the hardware and perform both measurements and data evaluation. The drivers for the filters are installed here, as is the

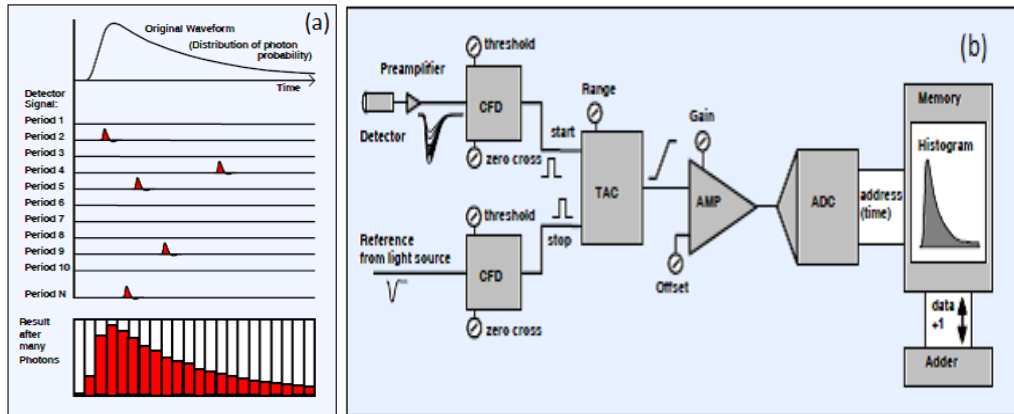


Figure 4.3: Principle of TCSPC. Repeating the same measurement several time and recording the time of a detected photon will create a histogram seen in (a). Illustrated in (b), the detection of photon will trigger charging of a capacitor, which is stopped with the arrival of a sync signal from the laser source. The voltage over the capacitor is proportional to the time between the two pulses, and this is converted to a position on a time histogram.[16]

spectrometers.

4.7.1 LUNDtofs program

LUNDtofs is a program made for the Lund biophotonics group, it can control both the filters and attenuators used while displaying the output from the TCSPC card, both as a histogram and as numerical value of counts per second. The program is also used to collect measured data and saving it with a specified file name. Parallel to this thesis, work was also done to improve the automated functions of the program, so that it could be given a wavelength range and then do measurements on the same sample with a set wavelength step size in that range.

The built in automation process lets the user design a wavelength range and a step size, then collects data for each step from start to stop. The automation also have variable settings for desired count rate and can increase integration time if needed to reach higher counts. It needs to calibrate the attenuation level for the time reference peak first, which is done with the sample arm blocked. Once the program knows what count rate is generated for a set attenuation, it can easily adjust the time reference peak when the actual measurements are run.

Figure 4.4 shows the program while performing an automated measurement. Top left is the automation control including the start wavelength, step size and stop. Further down is the manual measure controls and the save file designation. Bottom left the current count rate is displayed, in photons/second, an just above is the manual control for the attenuator.

At the right hand side is a histogram of the current measure, with two main peaks corresponding to the time reference and the sample. Below is the progress of the current 25 second measurement displayed as straight lines for

peak position, with the curved lines below representing the full automation scan. Notice that the peak positions have moved in time with changing wavelength.

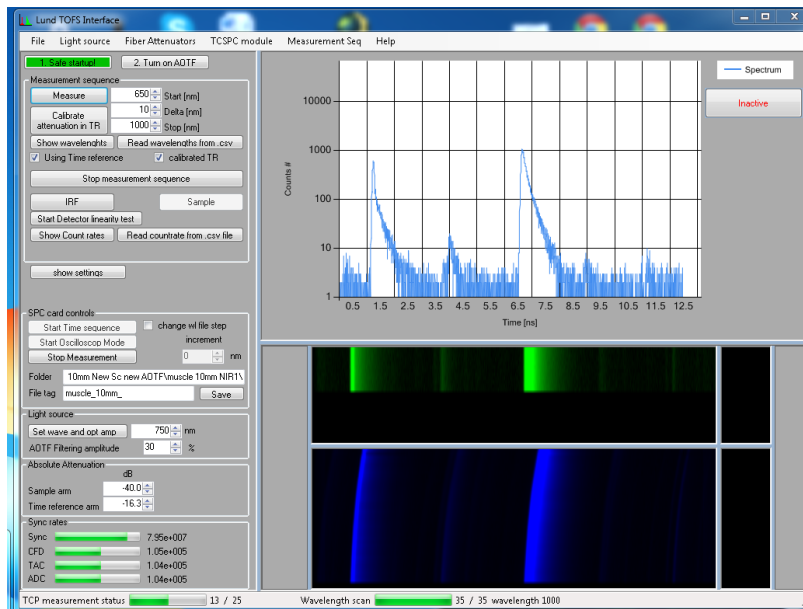


Figure 4.4: Main window of LUNDtofs program while automation is running

4.7.2 Timeresolved v3

Timeresolved is a Matlab program created for the LUND biophotonics group. It can import data files created by LUNDtofs program and perform curve fitting using both diffusion model and Monte Carlo. To help improve the curve fit there are several variables that can be modified, including what channels of the measured data is used, how large section of the curve the fit should try to match and how fine steps the iteration process should use. The software implements a Levenberg-Marquardt algorithm in Matlab that fits the data to the model, via minimizing the sum of the least squares of the deviations.

The program starts with importing the spectral files selected by the user. Then it tries to locate the peaks in the measurements, and removes incorrect ones known as outliers. It sums up the 25 sets collected for each wavelength and tries to find the best fit curve to the measurement points with the chosen model and settings. The resulting fitted curves are displayed graphically for evaluation, when the fit is accepted then the values of absorption and scattering can be saved to an output file.

5 New system setup

This part details the installation of the new system components and the evaluation of those compared to the existing setup. Two new components, the LLTF filter and the 10 W laser, is tested for functionality and stability, then they are compared to the old systems AOTF/NIR2, focusing on the performance of the two filters. The new AOTF VIS/NIR1 filter is only tested to insure that it is working. No evaluation between the old and new NIR1 is performed, they are assumed to be identical.

The work was performed and is presented in the following order. First the old system is rebuilt and tested. Next the performance of the new 10 W laser is compared to the 6 W laser. After this the LLTF is installed and put through a few initial tests to get familiar with the working procedures of the filter and what output to expect. Using the 10 W laser we then perform a series of measurements on different tablet samples using both the LLTF and the AOTF, the result of which then form the basis for the evaluation of the filter.

5.1 Rebuilding old system

Before unpacking the new components we started with rebuilding the old system as parts of it had undergone service, then ran several measurements on known samples to verify that it delivered results comparable to previous measurements. The 6 W laser and a AOTF filter were connected to the existing optical fibre layout and then to the detectors, before starting the computer and control software. All systems ran as expected so the laser was powered up and put into operation.

Figure 5.1 show comparison of select wavelengths for a sample of crushed BG36 filter. The test show that within a small error margin the systems give the same values for μ_a and μ'_s . This important step insures that all the optical components are working correctly, from here on no modifications are made to the rest of the system except for the switching of targets and detectors, changing the lasers and filters as required for the desired tests.

5.2 Installation of new components

The 10 W Fianium SC-480-10 laser and the LLTF are both bought new from the manufacturer, and arrive with fibre holders needed to incorporate them in the system. The drivers supplied are installed on the controlling computer, the system detected the new parts directly. No output fibre was supplied with the LLTF so one was selected in the lab.

5.3 10 W Laser SC-480-10

The new 10 W laser is expected to perform the same as the 6 W laser, with the exception of output power, since they both use the same technology to create the super continuous light. A short set of measures were done with both lasers to ensure this, using AOTF in NIR1 and the same BG36 sample as in the systems setup check. The results, found in Figure 5.2, show that the two laser do perform similarly.

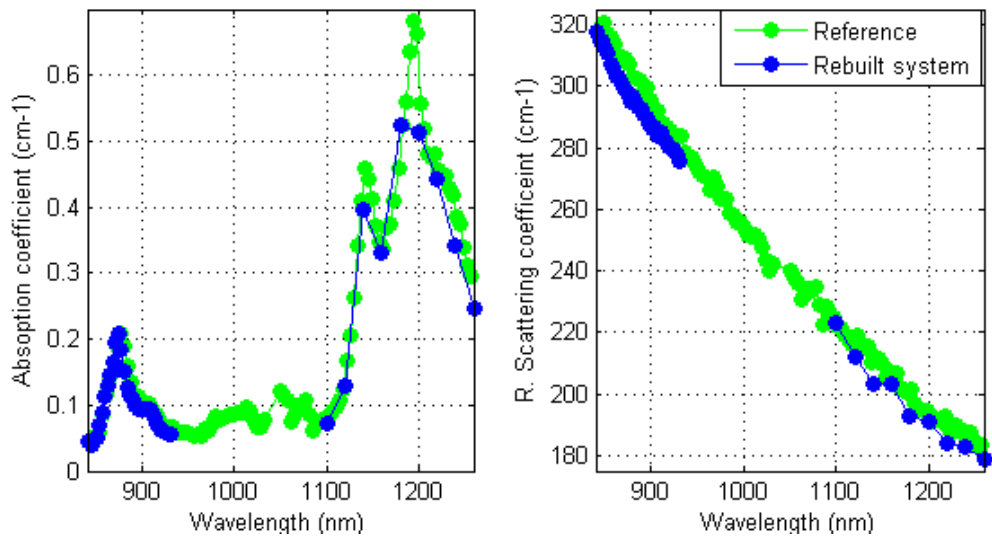


Figure 5.1: Comparing results of the rebuild system with reference data from [17]. Areas sampled are chosen due to the absorption features present, one for each detector range.

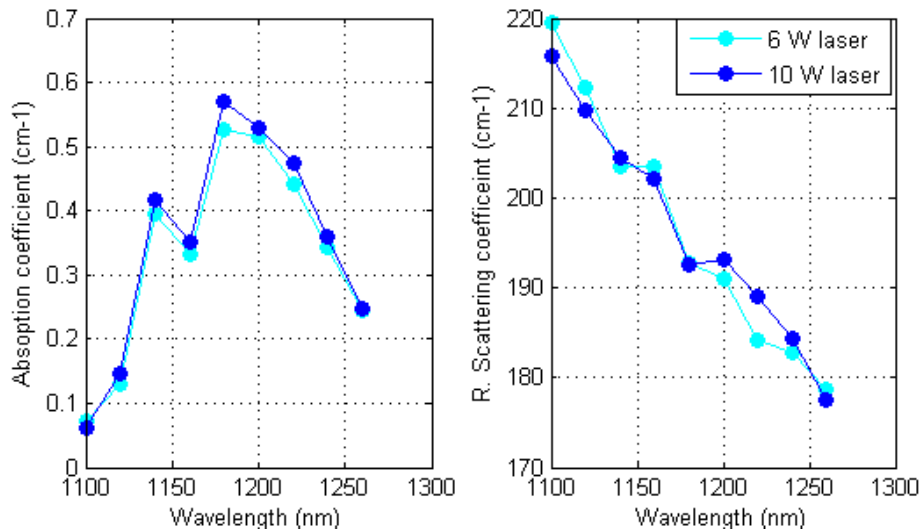


Figure 5.2: Comparing measurements taken on a 1.91mm BG36 sample, using a AOTF/NIR1 filter with the 6 W and 10 W lasers respectively.

5.4 LLTF

The LLTF is specified as having sharper resolution than the AOTF, in both time and frequency domains, it should also provide higher transmission efficiency. We therefore performed several measurements where the only changes made in the system are switching between the two filters to see if there are any detectable differences. All these tests are conducted with the 10 W laser as source.

5.4.1 General performance

After installing the LLTF a few initial test measurements were made to get a baseline of secondary parameters for the detection system, such as expected output power for attenuating purposes and the timing for the pulse signal from the laser to the counting card. During these measurements we noticed that the IRF signal peak were much broader for the LLTF than for the AOTF, which was unexpected as the LLTF was supposed to give less time distortion. We recorded the width of the IRF pulse at half peak height (FWHM) for the LLTF and AOTF filters, which supported our initial observation (see AOTF and LLTF multi mode in Figure 5.3). We realised that the output fibre selected from the lab was a standard multi mode fibre, and this was the cause of the broadening of the pulse. After changing to first a single mode fibre and later to a GRIN fibre, we found the LLTF to perform as well as or better than the AOTF in respect to pulse broadening, as can be seen in Figure 5.3.

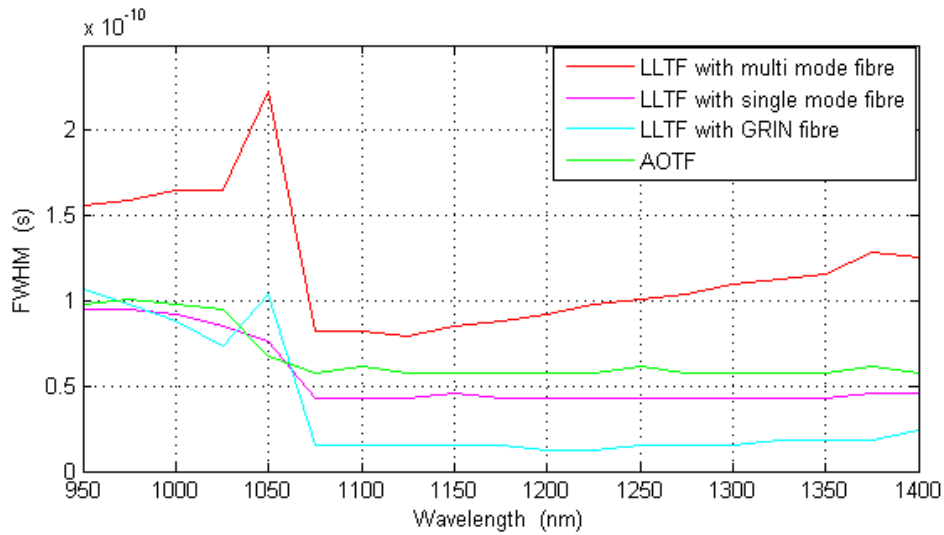


Figure 5.3: Full Width, Half Maximum for the IRF signal using the AOTF, and the LLTF with different fibres

5.4.2 BG36 measurements

Measurements were performed on the same sample that was used to validate the rebuilt system, a BG36 tablet that is 1.91mm thick. Data was collected for the LLTF and the AOTF with the 10W laser as the source, and can be seen in Figure 5.4. The curves follow each other closely, so for this setup there is no substantial difference between the filters, although a slight crossover from the absorption peaks can be seen in the scattering results for the AOTF.

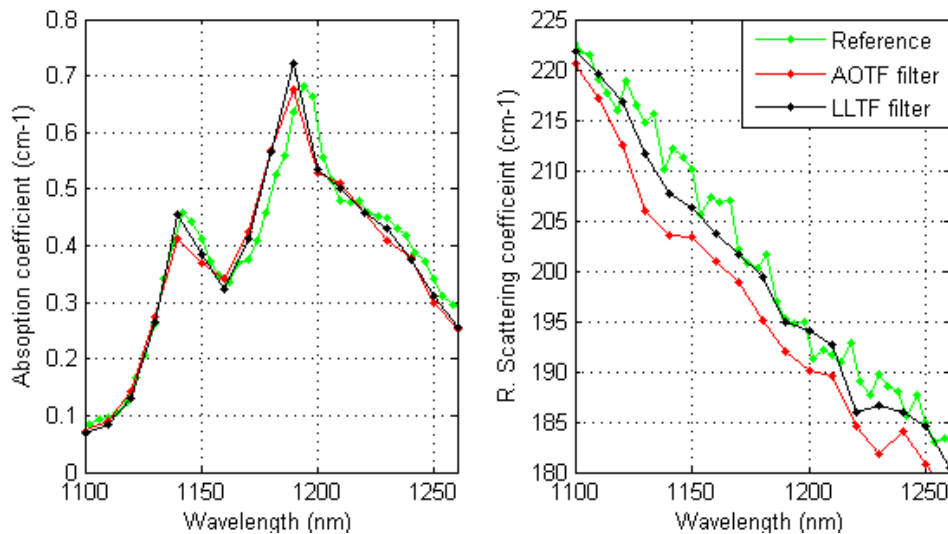


Figure 5.4: Comparing results from measures on a 1.91 mm thick BG36 sample, using the LLTF and AOTF filters. Data from [17] included as reference.

Next similar measurements were conducted on a BG36 sample that is 3.64 mm thick. The added pathlength that the light needs to travel through a thicker sample means that the effects of absorption will be higher. In Figure 5.5 we can see a marked decrease in the scattering for the AOTF near the peaks of the absorption curve, similar dips exist for the LLTF to a much lower degree. The difference is caused by the narrower spectral pulse width that the LLTF provides, meaning that the absorption peaks will have less effect on the data evaluation software.

5.4.3 N18ln2c measurements

A tablet containing a medical sample labelled N18ln2c were selected for a last set of test measures, to lessen the risk that the characteristics of the BG36 samples masks features that are caused by the filters. The results in Figure 5.6 show the two filters performing very similar, once again a slightly larger cross talk from the absorption peaks can be seen as dips in the scattering curve recorded with the AOTF.

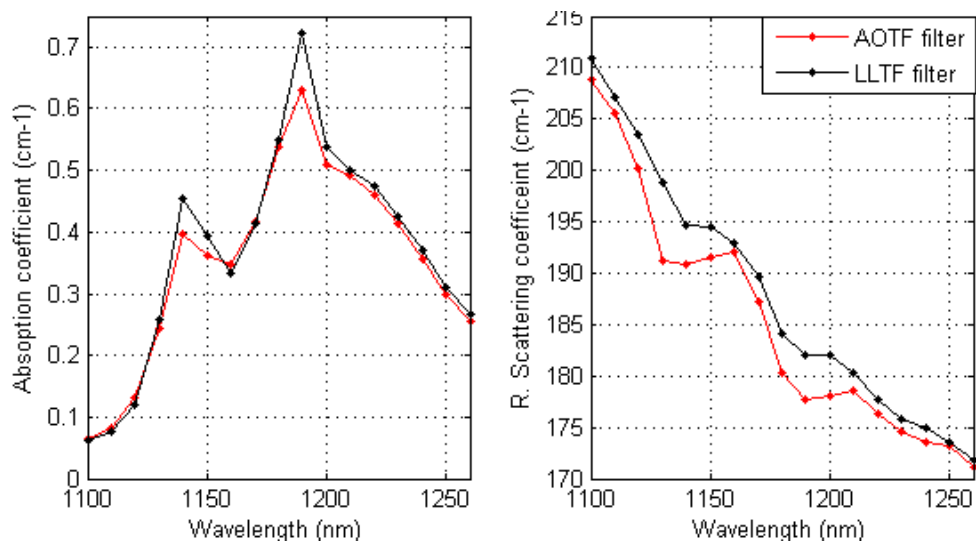


Figure 5.5: Comparing results from measures on a 3.64 mm thick BG36 sample, using the LLTF and AOTF filters. Note the higher absorption maxima for the LLTF and the larger dips in the scattering curve for the AOTF.

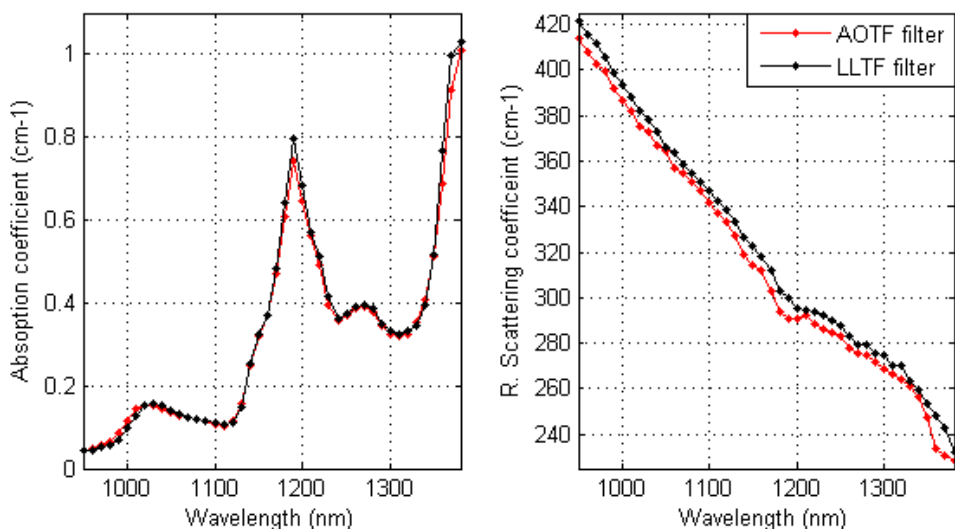


Figure 5.6: Comparing results from measures on a N18ln2c tablet sample, using the LLTF and AOTF filters. The absorption maxima can be seen to be higher for the LLTF, and there are larger dips in the scattering curve for the AOTF.

5.5 Comparing systems

The spectral resolution of the two filters could be compared using a spectrometer. Unfortunately the devices we had access to at the time for this thesis work did not have a sharp enough resolution to differentiate between the two filters, all effects were masked by the resolution of the spectrometer. Comparing the

measured samples we can see that the LLTF has less cross talk from absorption changes to the scattering curve, showing that the pulse is not as broad as the AOTF one. The values at absorption maxima are also higher for the LLTF, as is expected with a more narrow pulse.

The transmission efficiency of the LLTF was observed to be higher throughout the measurements. When setting the count rate to the desired level for measuring, usually $1 \cdot 10^5$ counts/second, the attenuation level had to be higher for the LLTF than for the AOTF. Also noted was that the count rate of the spectrometer used for aligning the fibre coupling to the filters were higher for the LLTF.

6 Muscle tissue measurement

The goal with the measurements in this section is to acquire a absorption and reduced scattering spectra from muscle tissue in vivo for the entire wavelength-range from 650 - 1340 nm. In this region several tissue components have strong absorption, with water dominating completely at higher wavelengths. With the absorption being so strong it is important to have as high a intensity as possible as input, to get a significantly high count rate passing through the sample to the detector. For this reason the 10 W laser and the LLTF filter was expected to give the best results.

6.1 Material and method

The tablet holder used in the testing of the system was removed and replaced with two optical fibres mounted in metal needles, with flat ends. This protected the fibre tips while facilitating the positioning of the fibres against the skin of the subject. The needles where fastened in a plastic holder and attached to the arm of the test person, using surgical tape and a Velcro strap as displayed in Figure 6.1. Before the measurements the area is covered with black cloth to minimize any background light affecting the data. The position on the arm was chosen with regards to avoiding underlying blood vessels and tendons if possible, and aligned along with the muscle fibre. The same subject was used for all the measurements in this thesis.

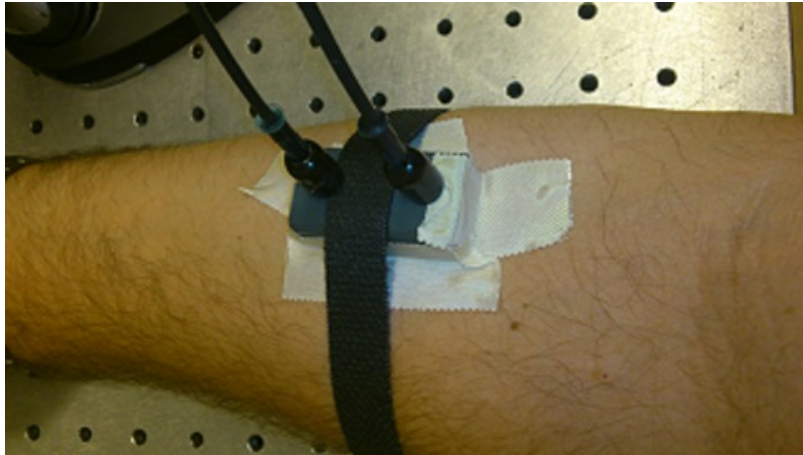


Figure 6.1: Optical fibres attached to the lower left arm of the test subject.

6.1.1 Data collecting and Evaluation

The measurements were performed using the LUNDtofs automated sampling ability. Automation was selected both for speed purposes and to facilitate the measures, as the main part of the data was collected with the test subject alone operating the system. Since the computer then only needs to be given start values and the measurements started, this allowed for a more comfortable

position for the subject. The only thing needed to be done during the recording was noting the count rate for IRF purposes. Many of the measurements are collected over the length of hours, with the subjects left arm kept in a fixed position.

The collected data was evaluated using both diffusion theory and Monte Carlo simulations. The diffusion model gave surprisingly accurate results throughout, compared to MC used as gold standard, even though the model was at the limits of its theoretical validity. The diffusion model requires the scattering to be significantly higher if it is to be valid, and the scattering and absorption were close in value, with absorption at times being higher. All data presented in this thesis are based on Monte Carlo simulation fits.

6.2 Results and discussion

6.2.1 Validating method

Data on the absorption and scattering spectra for muscle tissue can be found in the literature ([11, 12, 19, 20]), but not obtained using Time-of-Flight measurements above 1000 nm. The first measurements were conducted in the range of 650 nm to 1000 nm, using a AOTF in NIR1 range and the SPAD detector, recording the optical properties with 10 nm steps. The fibre separation was set at 20 mm, the same as the distance used for the studies in [12]. Comparing the results in Figure 6.2, we find that for the scattering spectra's there is good correspondence, the absorption also largely follow the data for the arm muscle sample with thinner layer of subcutaneous fat, although a higher absorption is seen throughout.

At the shorter wavelengths we can see the haemoglobin absorption that decreases rapidly, and then again have a small peak around 760 nm. The peak above 950 nm corresponds to the absorption of water. One can see this peak in the curve for Arm(thinner) from [12], but not as prominent as in our data. The first part of the peak (below 950 nm) is due to lipids in the subdermis, with an absorption peak around 920 nm, while water have a peak at 970 nm which show more prominently in muscle tissue [20]. The absorption coefficient at 970 nm for 100% water is close to 0.5 cm^{-1} , so in our data we are likely overestimating the absorption. While the reason for the high absorption values are not investigated fully, we estimate that the major effect comes from compression of the tissue.

The needle holder where pressed against the skin with the fibres protruding slightly, resulting in the tips pressing down on the skin and compressing it. This will alter the geometry, witch might influence the theoretically calculated values. For the MC simulation we use a semi-infinite plane with a straight boundary, but with the fibres pressing down this does not hold true. Fewer photons will be lost due to escape over the boundary, so more light with a shorter path length will arrive at the detector. This will alter the ratio of early photons versus late photons with longer path length, and the model would interpret this as higher value of μ_a .

Simulations were done with a MC model with an infinite geometry, and compared to the semi-infinite plane. The estimated absorption values were even higher in the infinite case. The compression does not protrude deep enough

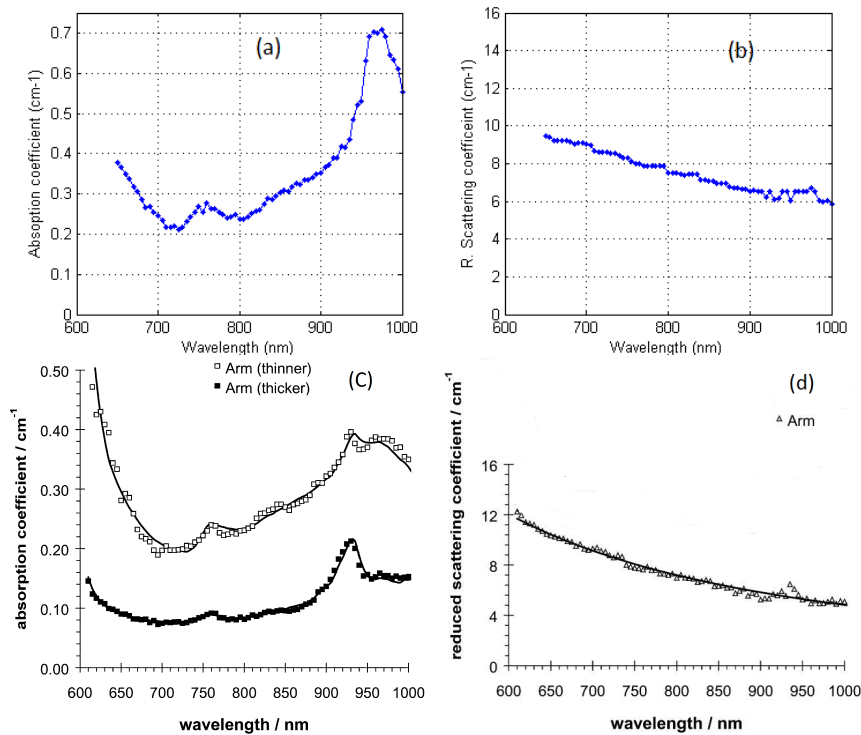


Figure 6.2: Muscle tissue spectra measurements with 20 mm fibre separation. There is good correspondence between the absorption in (a) with the reference Arm(thinner) in (c), except for the prominent water peak at 970 nm. The measured scattering in (b) is similar to the reference (d). [12]

so that no light is lost due to the boundary, once more the high ratio of early photons to late is seen as higher absorption.

The water absorption peak in the recorded spectrum presented in Fig. 6.2 was higher than other measures taken on the same subject, although all gave a more prominent peak relative to the lipids than the reference does. That absorption from water is high could be caused by several factors. Compression will alter the spectra and may result in increasing the absorption [21], and this may possible contribute to the enhanced water influence. In particular since the subdermis layer will be compressed more than the underlying muscle, the resulting optical path will increase for muscle tissue compared to the subdermis.

While care was taken to avoid blood vessels, it is possible that the sample area contain lower lying blood vessels. This would also increase the haemoglobin absorption. Another possible reason could be that the lipid content in the subject tissue is simply lower than the reference subjects, as a natural variance.

The amount of compression from the needles where difficult to control using the fibre holders available. Both the distance the fibre were protruding from the holder and how tightly it was secured to the arm contributes, and were not easy to reproduce in the measurements.

The fibres have caps that adds protection against background light interfering. When the needles are set in the holder they were pushed in until the protective caps where set against the base, and then secured with screws in this position. This was used as a guide to the needles being at the same position. However, the caps are movable and might have changed position on the needle between measurements. Directly measuring the length of the needle from the base of the holder were not possible, as it often had to be secured against the arm before the fibres where inserted. The holder is secured to the arm with both surgical tape and a Velcro strap. Some pressure is needed to keep the holder flat against the skin, the amount will vary for each occasion. Together with the slightly changing position of the needles makes it hard to control the amount of compression.

If the measurements were to be redone, a new procedure on securing the fibres to the skin would help. Most of the data was collected by the test subject alone in the lab, securing the holder and placing the fibres. One simple procedure change would be to have a subject other than the operator, enabling the fibres to be fastened in the holder before it is placed on the subject, so that the fibre distance can be more precisely controlled.

6.3 Optical properties above 1000 nm

The next step was to attain spectra above 1000 nm, using the LLTF filter and the PMT detector and fibre separation at 20 mm. It soon became apparent that the high absorption in these wavelengths resulted in very low count-rates of detected photons. To get high enough counts for the evaluating software to work, the integrating time was increased, from 1 second to 5 seconds. Since the LUNDtofs collects 25 samples for each wavelength, this resulted in each spectra taking many hours to acquire. Due to time constraints and to keep the test subject from having to sit in the same position for unduly long times, the step between samples of the recordings was changed from 10 nm to 20 nm.

Even with longer integration times the high absorption made collecting reliable data difficult, and several sets of measurements had to be discarded since the low count-rates prevented the Monte Carlo simulation to fit to the curves. Figure 6.3 show the best fitted results from the measurements. The absorption spectra looks as was expected with prominent peak at 1200 nm from both water and lipids, and the increase in water absorption above 1300 nm.

The reduced scattering starts out following the same approximate rate of decrease as before, but above 1200 nm it breaks of and starts to increase again. The dip at 1200 nm is likely due to cross talk from the absorption peak, making the scattering values look to be decreasing more rapid than they actually are and introducing a false increase as the dip ends. Above 1300 nm there is another increase in the scattering. This is believed to be due to a decrease in the anisotropic factor g , caused by the strong absorption peak of water with maxima at 1450 nm coupled with anomalous light dispersion of the tissue scatterers [19].

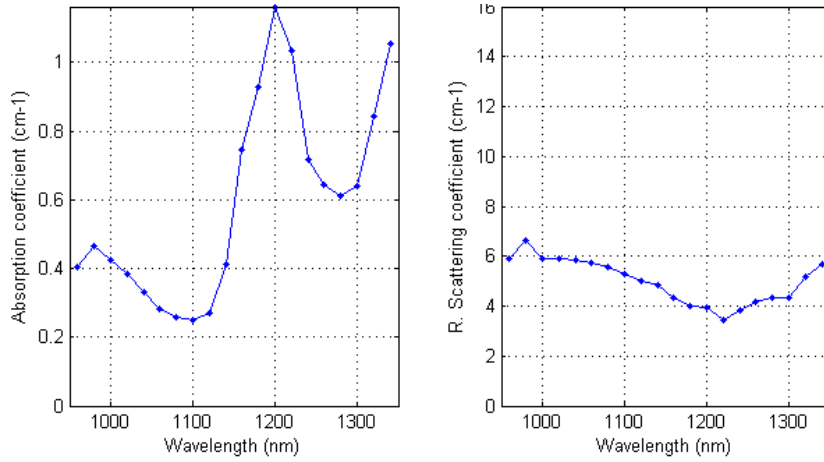


Figure 6.3: Absorption and reduced scattering spectra taken on arm muscle with 20 mm fibre separation, 960 - 1340 nm.

6.3.1 Shorter fibre separation

In an attempt to increase the count-rates, the separation of the fibres was decreased to 10 mm. This would enable more photons to reach the detector, both by shortening the optical path, and thereby the loss through absorption, and decreasing the spatial spread of the photons. The drawback is that the penetration depth will be smaller, and that the distance might not be long enough so that the light can be considered diffuse.

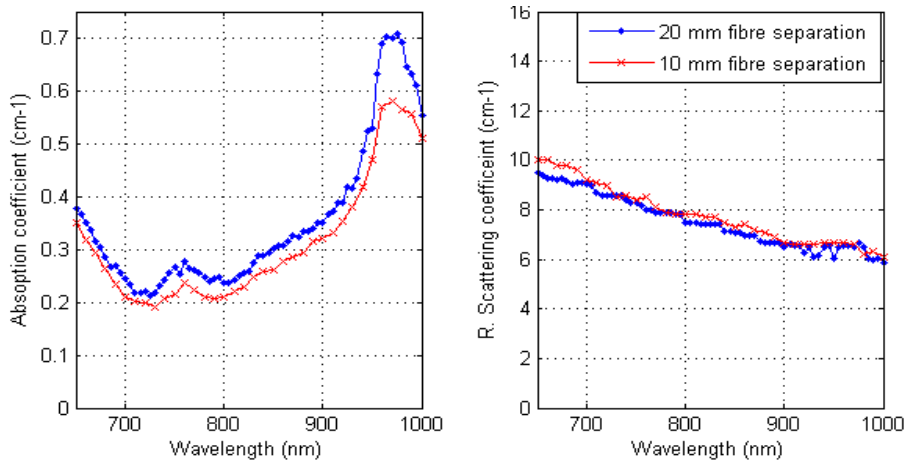


Figure 6.4: Comparing absorption and reduced scattering spectra recorded with 10 mm and 20 mm fibre separation, 650 - 1000 nm.

Measurements were performed with both the AOTF and LLTF with steps of 10 nm. Figure 6.4 show the result for 650 nm to 1000 nm, compared to the previous measures made with 20 mm fibre separation. Using Monte Carlo sim-

ulations for data evaluation we had no problems performing curve fits for these results, so the misgivings about the light becoming sufficiently diffuse can be discarded. The two absorption spectra have the same shape and features, but at a slight offset as the values are lower for the 10 mm measures throughout. This might be a result of less pressure from the fibres in this measurement and thus a stronger influence of the subcutaneous fat and less of the water, but this is mainly a conjecture. The scattering results show good correspondence.

Fitting the measured spectra for the LLTF proved to be more troublesome. While the MC simulation had no problem with reproducing the height of the curve, it could not manage to fit the curves in time domain resulting in clearly erroneous scattering results. The solution was to introduce a time delay for the IRF results, thereby shifting the histograms in time and enabling a good fit. Figure 6.5 show two histograms, with and without the time shift. The red curve from the theoretical model should overlap the dotted blue measurement data for a good fit. The introduced delay can be seen in the shift of channels for the shaded curve that represents the IRF measurement.

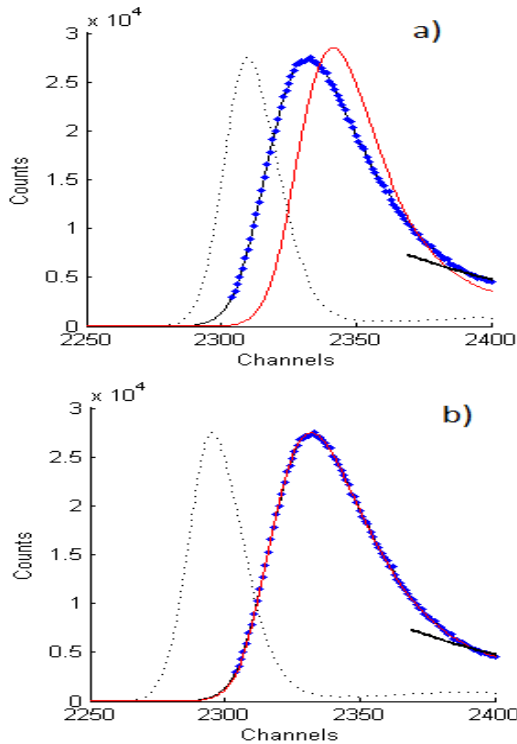


Figure 6.5: Two curve fits on the same data, where (a) is unmodified while (b) have a delay of 44 ps introduced for the IRF. The blue dotted curve is the measured data and the red curve is the computed theoretical model. For a good fit they should overlap. Notice the shift in the shaded IRF curve between (a) and (b). Each channel represents 3 ps.

The source of this timing error is unclear, no other measurements using the same setup has shown a similar shift. The delay value that gave the best fit was 44 ps, meaning that an error in the optical pathways are unlikely as the light would travel over one centimetre during that time. The only changes in the optical path between the measurements are moving the fibre from the arm holder to the holder for the black paper used in the IRF measurement. While

small errors could be made coupling the IRF holder, such large distances as one centimetre are not likely.

Another source for the error might lie in the electric start signal from the laser, used for timing purposes. Either the laser sync was slightly off or the counting card introduced an error. As the laser was turned off for a short break between the arm measurements and the IRF, it is possible that some timing error was introduced when restarting it.

The result for the LLTF filter recording is shown in Figure 6.6 together with the previous data from 20 mm separation measures. Looking at the absorption from 950 nm to 1000 nm, we see higher values than for 20 mm, but the result are very close to the values for the 10 mm separation curve in Figure 6.2.

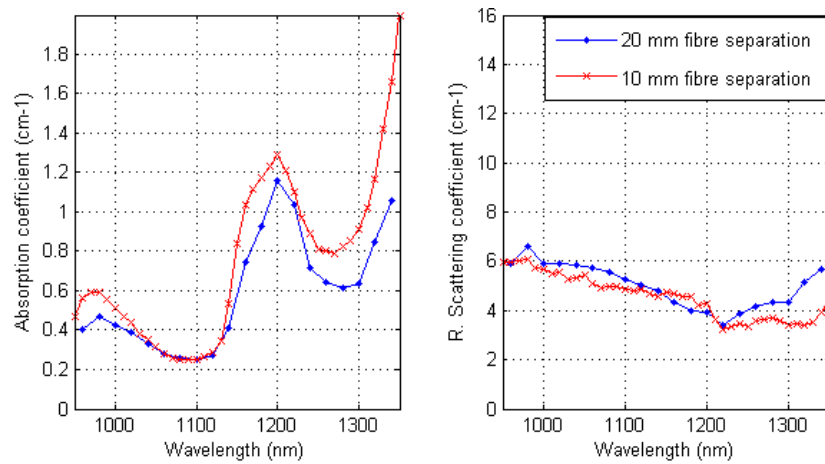


Figure 6.6: Comparing spectra taken with 10 mm and 20 mm fibre separation, 960 - 1340 nm.

Overall the absorption curves in Figure 6.6 looks similar. The peak at 1200 nm is broader for the 10 mm measurements, corresponding to higher contribution from lipids with an absorption peak at 1210 nm. As the light won't penetrate as deep into the tissue for the 10 mm fibre distance, the subdermis fat layer contributes more than with 20 mm distance.

The scattering spectra for the two measurements give the same general result, with the same approximate decrease rate and starting to increase as the water peak hits in above 1300 nm.

6.3.2 10 mm spectra

Figure 6.7 show the combined measurements with 10 mm fibre separation, from 650 nm to 1350 nm. Below 800 nm we can see the deoxyhaemoglobin absorption that is dominating, with the sharp decline below 700 nm and the small peak at 760 nm. Oxyhaemoglobin adds absorption with a broad maxima around 900 nm that continues over into the peak for lipids at 920 nm and water at 970 nm. In these measurements the effect of the lipids are hard to see as the water absorption masks them and the resolution is not sufficiently good to resolve the peaks. At 1200 nm we see a broad peak arising from several different substances. Lipids have a peak at 1210 nm, while water, elastin and collagen all have absorption maximums at 1180 nm. While we cannot resolve the peaks in these measurements there is a hint of the first peak at 1180 nm as a disturbance on the larger peak. With better resolution, by making measurements with smaller steps and increasing integration times for each step, it might be possible to distinguish between the two.

Above 1300 nm the absorption of water increases drastically. The Time-of-Flight system used here is not able to produce measurable responses much above 1350 nm as the absorption in tissue is too high. Using the 10 mm separation it was possible to get results up to 1370 nm, but as amount of light passing through was very low they were very noisy and difficult to produce good fits for. The measured absorption continued to rise as expected, and as the high values would drown out any other features if put in a plot it was decided not to include them in the data presented here.

Comparing the values for absorption and scattering for the higher wavelengths we can also see that they are starting to be of the same order of magnitude, and for wavelengths above 1350 nm then μ_a might be even larger than μ'_s . As the diffusion theory uses the approximation that $\mu'_s \gg \mu_a$ this is a problem. The MC simulations are able to reproduce the curves despite this, but attempts to use the faster Diffusion model fail completely. For this reason MC simulation were used exclusively for all computations on the muscle tissue measurements.

The low scattering presented a problem when choosing fibre separation. If the fibres are placed closer together, the average pathway for the detected photons are shorter, and fewer will have been absorbed. However, the chance of scattering will also be low and if the fibres are placed too close then the light arriving cannot be considered diffuse, as the photons won't have been scattered multiple times. A rule of thumb is that the fibre distance d should not be smaller than the inverse of the scattering coefficient μ'_s , i.e. $d > 1/\mu'_s$. At the longer wavelengths we are approaching this situation, but as μ'_s doesn't go below 3 cm^{-1} then at a fibre separation of 10 mm it is still reasonable to consider the light diffuse.

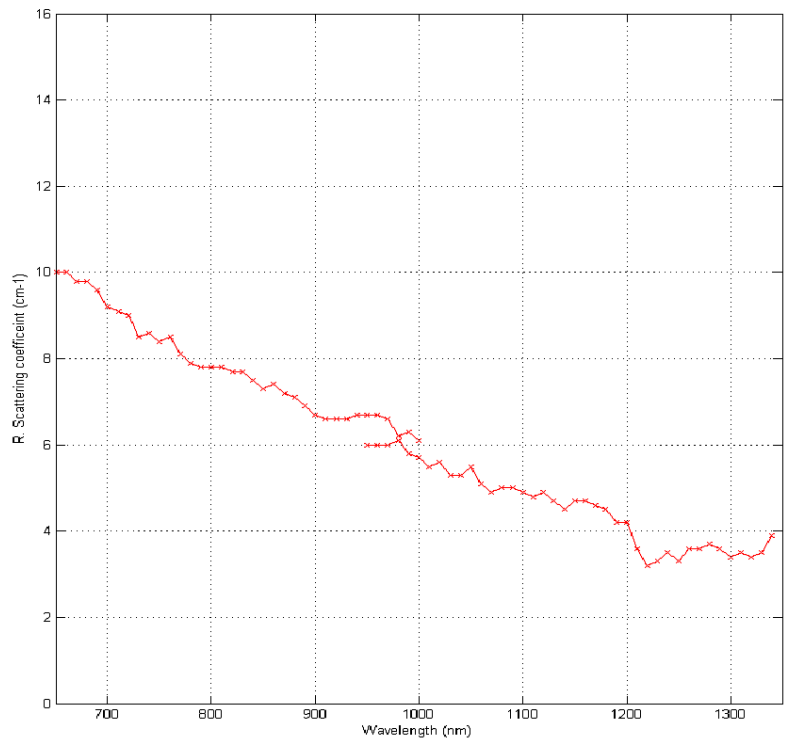
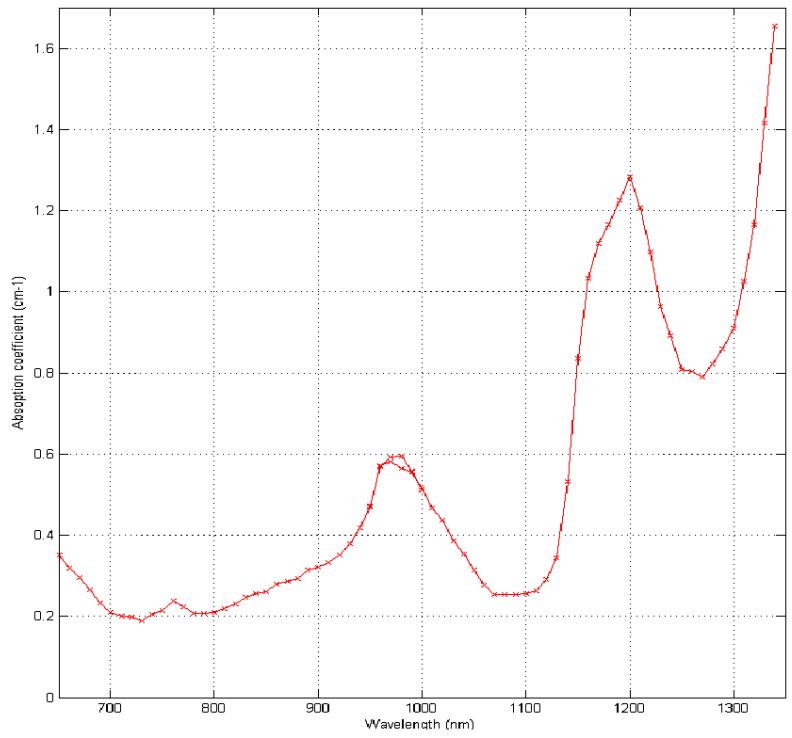


Figure 6.7: Spectra for absorption and reduced scattering coefficients of muscle in lower arm, taken with 10 mm fibre separation. 650 nm - 1340 nm

7 Concluding remarks and Outlook

Here some conclusions of the project are presented, starting with the aim of the work. After this a outlook and suggestions for further work are followed by a personal reflection.

7.1 Aims

The laser installation went smoothly and it is easy to use. The main difference from the old laser, apart from the higher power, is that it has an internal power supply that requires less warm up time to be stable than the stand alone supply of the old laser. It has more features, but most of those are not used or needed for our setup.

The laser started to loose output power randomly just shy of a month after delivery. The problem was diagnosed remotely, but resulted in the laser being shipped back to the manufacturer together with the new filters for repairs. The error was fixed and the laser was stable for the rest of this work.

The LLTF filter is shown to have better resolution than the old AOTF, it therefore produce more accurate absorption values and it is less susceptible to scattering results being affected when the absorption changes rapidly. It also have better throughput ratio than the AOTF. The only perceived disadvantage is that there is no possibility to close all throughput remotely, light is always transmitted once it is put into operation. The AOTF can be used as a shutter by specifying zero transmission. This doesn't impede the actual measurements, only adds extra steps to insure laser safety.

Acquiring the absorption and scattering spectra for muscle tissue proved to be difficult. As the new 10 W laser had to be shipped back together with the new filters (both LLTF and the VIS/NIR1 AOTF), we were left with only the old 6W laser, and the NIR1/NIR2 AOTF that had just returned from being repaired. We started in the NIR1 range (650 nm - 1000 nm) since the absorption was assumed to be lower there. Unfortunately it soon became apparent that the NIR1 crystal was not working properly, this had not been discovered previously since all the measurements had been done with the new VIS/NIR1 filter. Switching over to the NIR2 we were able to get some results, but the count-rate were low at the absorption maxima. Since the reference data had been acquired with 20 mm fibre separation, we had decided to keep the same distance and relied on the more powerful laser to be able to produce better throughput. With the hopes of speedy return of the new laser we therefore decided to wait before doing further measurements, the end result being that we had very limited time to acquire the data.

It has been shown in this thesis that it is possible to produce a spectra over the optical properties for human muscle tissue from 650 nm to 1350 nm with the pTOFS system. Measurements were made up to 1370 nm, but the high absorption made it difficult to do a good model fit so they were left out of the presented data. The results give good correspondence to previous work, although the absorption is slightly high. This is thought to be an effect of the fibre tips pressing down on the skin, compressing the tissue.

7.2 Outlook

Human tissue is highly scattering so conventional optical absorption detection techniques does not work. Time-of-Flight Spectroscopy give a way to measure both the absorption and the reduced scattering coefficients for tissue in a non-destructive way, it could possibly be used in clinical situations on live subjects.

The limited time left no room for several additional measurements that we would have liked to carry out, and that are left for future projects. It would have been valuable to do repeat measurements on the same subject to ensure that the results are consistent, also it would have been interesting to measure on several different subjects.

While increased integration time results in the measures taking longer time, it also give better data for the low count-rates at high absorptions. It could be possible to get better resolution of the high absorption peak at 1200 nm, to distinguish between water and lipids, if measurements where made with shorter wavelength step and longer integration times.

One of the main uncertainties in the results comes from the compression of the tissue due to the pressure from the fibre tips. Improved holder together with a better procedure on how to place the fibres should reduce this complication, having someone other than the subject himself place the fibres would help. It would also be interesting to see if it possible to measure the effect, how much does the absorption actually change due to pressure from the needles.

Muscle tissue is highly fibrous, with long fibres lying parallel to create the muscle. All the measurements in the thesis have been carried out along the length of the fibres, but it could perceivably be that both the absorption and scattering spectra change depending on if the probes are parallel or perpendicular to the fibrous tissue. This is something that should be explored in further experiments.

7.3 Personal reflections

During this project I have got experience in reading scientific literature and extracting the information I need for my work. My understanding of the theory behind light propagating in turbid media have increased, as have my knowledge of how to model data with MC simulations. I have also learned how to search for error sources in both recorded data and in laboratory hardware. Furthermore I have learned how to write a scientific paper, and how to use L^AT_EX. My understanding of how a university department work and is organized has benefited from the interaction with all the great people I've met here, often centred around the coffee machine.

Looking back, I would have liked to have more time to do measurement as I had no opportunity to correct errors that were found. There were work ongoing on three theses simultaneously, sharing the same limited lab time after the laser got back, and I should have made sure we scheduled our work better.

8 Acknowledgements

First of all, I would like to thank my supervisors Dmitry Khoptyar and Professor Stefan Andersson-Engels. Without your help and guidance this work would not have been possible.

A very special thanks go out to Sören Johansson, who collaborated with me on setting up the system and evaluating the new components. Having you around the lab answering questions about the Time-of-Flight system and walking me through the procedures sped up my understanding considerably.

Another special mention go to Karolina Dorozynska for the time spent in the lab and your assistance in some of the muscle measurements.

I would like to thank all members in the Biophotonics group for creating such a warm and supporting working environment, and to the Atomic Physics Division as a whole for the interesting time. Special note go to Anne and Harriet for keeping me in touch with the real world.

Most importantly I would like to thank my wife, for her support and encouragement during my labours to finish my Master's Degree.
I love you Sara.

References

- [1] T. Svensson, *Pharmaceutical and biomedical applications of spectroscopy in the photon migration regime*. PhD thesis, Lund University (2008).
URL <http://atomic.physics.lu.se/biophotonics>
- [2] A.A. Subash, *Wide-Bandwidth Time Of Flight Spectroscopy Of Turbid Media*, Master's Thesis, Lund University (2012).
- [3] D. Khoptyar, S. Johansson, S. Strömblad, S. Andersson-Engels, *Broadband photon time-of-flight spectroscopy as a prospective tool in biomedicine and industrial process and quality control*, Spectroscopy Europe VOL. 26 NO. 3 (2014)
- [4] A. J. Welch and M. J. C. van Gemert, *Optical-Thermal Response of Laser-Irradiated Tissue*, (Springer, 2011).
- [5] J. Swartling, *Biomedical and atmospheric applications of optical spectroscopy in scattering media*, PhD thesis, Lund University (2002).
- [6] M. S. Thompson, *Photodynamic Therapy Utilizing Interstitial Light Delivery Combined with Spectroscopic Methods*, PhD thesis, Lund University (2004).
- [7] L. V. Wang and H-I. Wu, *Biomedical Optics: Principles and Imaging*, (Wiley, 2007).
- [8] Fianium Ltd, URL <http://www.fianium.com/>
- [9] *Introduction to Tissue Optics*, Hochschule Koblenz
URL <http://www.hs-koblenz.de/en/rac/fachbereiche/mut/forschungsprojekte/labore/labor-fuer-biomedizinische-optik/forschung/introduction-to-tissue-optics/>
- [10] T. J. Allen, A. Hall, A. P. Dhillon, J. S. Owen, P. C. Beard, *Spectroscopic photoacoustic imaging of lipid-rich plaques in the human aorta in the 740 to 1400 nm wavelength range*, J. Biomed. Opt. 17(6)(2012)
- [11] A. N. Bashkatov, E. A. Genina and V. V. Tuchin *Optical properties of skin, subcutaneous, and muscle tissue, a review*, Journal of Innovative Optical Health Sciences Vol. 4, No. 1, 9-38, (2011)
- [12] P. Taroni, A. Pifferi, A. Torricelli, D. Comelli and R. Cubeddu, *In vivo absorption and scattering spectroscopy of biological tissues*, Photochem. Photobiol. Sci. 2, 124-129 (2003)
- [13] A. Shaharin, *Photon time-of-flight and continuous-wave near-infrared-spectroscopy of human skeletal muscle tissue; a comparative study*. Master's thesis, Lund University (2013).
- [14] S. Marcet, M. Verhaegen, S. Blais-Ouellette, and R. Martel, *Raman Spectroscopy Hyperspectral Imager Based on Bragg Tunable Filters*, Université de Montréal (2012)

- [15] Micro Photon Devices,
URL <http://www.micro-photon-devices.com>
- [16] W. Becker *The bh TCSPC Handbook, 5 ed*, Becker & Hickl GmbH,
URL <http://www.becker-hickl.de>
- [17] Data collected by A.A. Subash, Lund University (2012).
- [18] S. Feng, F-A. Zeng and B. Chance, *Photon migration in the presence of a single defect: a perturbation analysis*, Applied Optics, Vol. 34, Issue 19, pp. 3826-3837 (1995)
- [19] A. N. Bashkatov¹, E. A. Genina, V. I. Kochubey and V. V. Tuchin *Optical properties of human skin, subcutaneous and mucous tissues in the wavelength range from 400 to 2000nm*, Journal of Physics D: Applied Physics 38 (2005)
- [20] C. R. Simpson, M. Kohl, M. Essenpreis, M. Cope, *Near-infrared optical properties of ex vivo human skin and subcutaneous tissues measured using the Monte Carlo inversion technique*, Phys. Med. Biol. 43 (1998).
- [21] E. K. Chan, B. Sorg, D. Protsenko, M. O'Neil, M. Motamedi, and A. J. Welch, *Effects of Compression on Soft Tissue Optical Properties*, IEEE Journal of Selected Topics in Quantum Electronics 01 (1997)

A Detailed schematic of the setup

